The Structure of Colloidal Quantum Dots from Dynamic Nuclear Polarization Surface Enhanced NMR Spectroscopy

Laura Piveteau,[†‡] Ta-Chung Ong,[†] Aaron J. Rossini,[§] Lyndon Emsley,[§] Christophe Copéret*[†] and Maksym V. Kovalenko*[†‡]*

[†] Department of Chemistry and Applied Biosciences, ETH Zürich, Vladimir Prelog Weg 1-5, CH-8093, Switzerland

[‡]Empa-Swiss Federal Laboratories for Materials Science and Technology, Dübendorf, Überlandstrasse 129, CH-8600, Switzerland

[§]Institut des Sciences et Ingénierie Chimiques, Ecole Polytechnique Fédérale de Lausanne (EPFL), 1015 Lausanne, Switzerland

KEYWORDS: Nanocrystals, Quantum Dots, Semiconductors, Colloids, Dynamic nuclear polarization, solid-state NMR

ABSTRACT

Understanding the chemistry of colloidal quantum dots (QDs) is primarily hampered by the lack of analytical methods to selectively and discriminately probe the QD core, QD surface and capping ligands. Here we present a general concept for studying a broad range of QDs such as CdSe, CdTe, InP, PbSe, PbTe, $CsPbBr_3$, *etc*., capped with both organic and inorganic surface capping ligands, through dynamic nuclear polarization (DNP) surface enhanced NMR spectroscopy. DNP can enhance NMR signals by factors of 10-100, thereby reducing the measurement times by two-to-four orders of magnitude. 1D DNP enhanced spectra acquired in this way are shown to clearly distinguish QD surface atoms from those of the QD core, and environmental effects such as oxidation. Furthermore, 2D NMR correlation experiments, which were previously inconceivable for QD surfaces, are demonstrated to be readily performed with DNP and provide the bonding motifs between the QD surfaces and the capping ligands.

TOC Graphics:

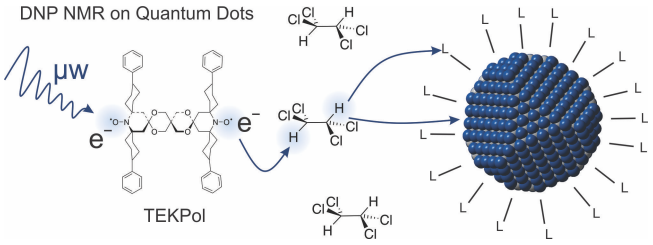

Introduction

Colloidal semiconductor nanocrystals, commonly referred to as quantum dots (QDs), exhibit size-tuneable optical and electronic properties and have become important as luminescent labels in life sciences[1, 2] and as building blocks for optoelectronic devices (solid-state lighting, photovoltaics, photodetectors and electronic circuitry).[3, 4] QDs are complex entities comprising an inorganic crystalline core, surface atoms and surface capping ligands.[5] Adjustments of the QD surface chemistry control the optical properties of individual QDs as well as the charge and the energy transfer in assemblies of QDs, and allow for their integration into solid-state devices and versatile bio-functionalization. Importantly, QDs are highly dynamic and reactive objects, in both their core regions (*e.g.* with polymorphism, and rapid chemical transformations via oxidation, reduction, galvanic or ion-exchange, or self-purification from impurity atoms, *etc*.) and at their surfaces (*e.g.* surface reconstruction, ligand adsorption-desorption, *etc*). It is therefore not surprising that structural characterization and the atomistic description of QDs remains a formidable challenge. In principle, nuclear magnetic resonance (NMR) spectroscopy would be the method of choice because of its ability to characterize molecules, solids, surfaces and interfaces. Both solid-state magic-angle spinning nuclear magnetic resonance (MAS NMR) and solution NMR investigations of sub-10 nm colloidal QDs (CdSe, CdTe, InP and PbSe, *etc.*) have provided information about the internal structure of the QD cores[6-9] and about the organic ligand capping, including the QD-ligand-binding equilibria in the liquid state.[9-13] However, both approaches have intrinsic limitations with respect to the chemistry of QDs. Solution NMR provides accurate information about the structure and binding equilibria of molecular species such as QD capping ligands, but is essentially blind to surface-bound ligands due to their slow and non-uniform tumbling. In the solid state, direct excitation MAS NMR records signal from all species present in the sample, with the principle possibility to yield insight specific to the atomic

structure of the QD surface and capping ligands *via* surface selective cross-polarization MAS (CPMAS) experiments.[14] However, CPMAS experiments on QDs are highly challenging due to the low concentrations of surface sites, the residual ligand dynamics that reduce hetero-nuclear ^{1}H-X dipolar couplings,[7] and most importantly, the generally poor sensitivity of NMR spectroscopy. From the QD chemistry point of view, NMR characterization should ideally be carried out directly on colloidal dispersions of QDs to rule out the effects of the isolation and purification procedures on the surface composition and surface coverage of the ligands. This challenge becomes even more daunting when considering that pristine QD colloids contain only milligram quantities of QDs, and the surface atoms and the stabilizing ligands constitute an even smaller fraction of the sample. To become practically useful, solid-state NMR of dispersed colloids of QDs requires orders of magnitude increase in the measured signal.

In the past twenty years, *in situ* high-field dynamic nuclear polarization (DNP) enhanced MAS NMR spectroscopy has become an extremely powerful method to enhance NMR signals *via* microwave (μw) induced polarization transfer from unpaired electrons of a radical polarizing agent to nuclear spins.[15, 16] With typical enhancement factors (ε) of 10-100, and corresponding shortening of the measurement times by two-to-four orders of magnitude ($\propto \varepsilon^2$), DNP enhanced NMR experiments may open new avenues for studying inorganic materials containing unreceptive NMR nuclei, such as QDs. Indeed, in the recent years, DNP enhanced NMR studies, exploiting unreceptive NMR nuclei such as ^{13}C, ^{15}N, ^{17}O, ^{29}Si, ^{59}Co, ^{119}Sn, have focused on inorganic surfaces and surface-bound molecules, providing enhanced spectra from surface atoms, including sub-surface atomic layers of the material.[17-27] DNP surface enhanced NMR spectroscopy should thus be uniquely suited for colloidal QDs, which are usually just 3-10 nm large and have high surface areas, and therefore can be polarized as a whole, allowing simultaneous and discriminative studies of the QD cores, surfaces and capping ligands; all in

colloidal solutions, and without the need for invasive isolation and purification procedures. Virtually all known colloidal QD materials and their organic- and inorganic ligand capping layers contain NMR active nuclei that potentially can benefit from DNP enhancement, including spin ½ nuclei (^{31}P, ^{77}Se, $^{111/113}$Cd, ^{115}In, $^{117/119}$Sn, ^{125}Te, ^{207}Pb, *etc.*) and also quadrupolar nuclei (nuclear spin > ½,^{133}Cs, ^{115}In, ^{17}O, ^{67}Zn, *etc*).

Here we demonstrate how DNP enhanced NMR can provide unprecedented information about the structure of colloidal QDs, kept in the original colloidal state in the amount of just few milligrams. We obtain high signal enhancement factors of up to 80, corresponding to gains in acquisition times up to a factor 6400. Such efficient polarization results from the homogeneous dispersion of biradical polarizing agents and QDs in mesoporous silica (meso-SiO_2) and is readily obtained for all common QD materials such as CdSe, CdTe, InP, PbSe, PbTe, and $CsPbBr_3$, and stabilized by all kinds of surface functionalities (inorganic or organic, charge and steric stabilization) and dispersed in any suitable polar or apolar solvent. New insights specific to the structure of QDs were obtained with DNP enhanced 1D NMR spectra. For a canonical QD system – CdSe QDs – we present the first direct evidence for the core-shell CdSe-CdX_2 (X=oleate, phosphonate) morphology, by resolving bulk and surface Cd and Se atoms with ^{113}Cd and ^{77}Se DNP enhanced spectra. Similarly, InP QDs are seen to exhibit clearly resolvable core and surface ^{31}P DNP enhanced signals. ^{125}Te DNP NMR spectra point to massive differences between CdTe and PbTe QDs. CdTe QDs are seen to remain un-oxidized even upon prolonged storage at ambient air, whereas PbTe QDs are found to comprise exclusively Te-oxide species at their surfaces, even with cautious air-free handling. To show new horizons for unreceptive quadrupolar nuclei, we show DNP enhancements of ^{133}Cs NMR spectra from perovskite $CsPbBr_3$ QDs. Previously inconceivable 2D correlation experiments can also be readily accomplished owing to strong signal enhancements, as demonstrated here for CdSe QDs with a 2D dipolar-

HMQC ^{13}C-^{111}Cd correlation spectrum, which reveals the identity of Cd atoms to which carboxylate ligands bind as a single surface moiety.

Experimental Section.

Synthesis of QDs. Organic-capped InP, W-CdSe, ZB-CdSe, PbSe, PbTe, CdTe QDs were synthesized and purified according to previously reported protocols, with slight modifications as detailed in Supporting Information. Care was taken to remove excess of ligands in the colloidal solutions used for DNP NMR experiments. Inorganic capped InP-S^{2-} and CdSe-Se^{2-} QDs were prepared via ligand-exchange reactions, as described by Nag *et al*.[28]

Conventional solid-state MAS NMR experiments. Solid-state NMR experiments at ambient conditions were performed on two Bruker spectrometers (11.7 T and 17.6 T) equipped with 2.5 mm and 4 mm two-channel solid-state probe heads and Avance III consoles, while spinning between 0.6-20 kHz. Low temperature experiments were conducted on a commercial 14.1 T Bruker instrument equipped with an Avance III console and a double resonance 3.2 mm low temperature MAS probe using MAS spinning of 10 kHz. Chemical shifts were referenced to 85% H_3PO_4 in H_2O (^{31}P), Me_2Se (^{77}Se), Me_2Cd (^{113}Cd) and 0.1 M aqueous CsCl (^{133}Cs).

DNP surface enhancedexperiments. DNP NMR spectra were acquired on two Bruker DNP NMR spectrometers (9.4 T and 14.1 T) equipped with Avance I and III consoles, and 263 and 395 GHz gyrotron microwave sources, respectively.[29] Double and triple 3.2 mm low temperature MAS probes were used in combination with 3.2 mm sapphire rotors.[29] For DNP NMR experiments, 1-4 mg of QDs were dispersed in 15-20 μL solution of biradical (16 mM TEKPol in TCE or 8 mM AMUPol in DMSO-d^6/H_2O/D_2O). This QD-biradical solution was either loaded directly into the rotor for reference experiments without meso-SiO_2 or, for one-step filling method, the meso-SiO_2 powder was impregnated with the QD-biradical solution on a watch glass,

then transferred into a rotor. The mass ratio of meso-SiO_2 to QDs has been optimized for each system, as illustrated for MSU-H meso-SiO_2 and InP QDs in Figure S2. In a two-step method, the QD dispersion was first impregnated into the meso-SiO_2 host, and dried, followed by impregnation of the biradical solution, aiming at the same overall amounts of QDs and biradicals as in one-step method (see Supporting Information for further details of NMR measurements and sample preparation). Chemical shifts were referenced to Me_4Si (^{1}H, ^{13}C), 85% H_3PO_4 in H_2O (^{31}P), Me_2Se (^{77}Se), Me_2Cd ($^{111/113}Cd$), Me_2Te (^{125}Te), 0.1 M CsCl in H_2O (^{133}Cs).

Results and Discussion.

DNP enhanced NMR of QDs using meso-SiO_2 matrix. The basic principle of DNP enhanced NMR experiments on colloidal QDs is outlined in Figure 1: the paramagnetic polarizing agent (here a nitroxide biradical) is dispersed in a suitable solvent (here TCE) and then brought into contact with the sample. Microwave (μw) irradiation transfers the polarization of the electron spins to the protons of the solvent and of other proton-containing molecular species residing at the QD surface. The enhanced proton polarization is then transferred through a CP step[30] to the desired hetero-nuclei. For QDs the range of this transfer from the surface is such that nuclei residing in the capping ligands, the QD surface or even the QD core are hyper-polarized.

However, *in situ* DNP NMR experiments are conducted at rather low temperatures, typically around 100 K to slow nuclear and electron relaxation.[15, 16, 31] In addition to the DNP effect, thermal (Boltzmann) enhancement of the NMR signal potentially contributes a factor 2.8 to the sensitivity at 100 K as compared to room temperature (RT). *The straightforward approach of mixing solutions of QDs and biradicals has proven to yield little or no enhancement.* This is because colloidal dispersions of QDs usually aggregate and precipitate upon cooling, or even at

room temperature in some cases, leading to phase separation from the biradical polarizing agent, and obliteration of the DNP effect. This aggregation can be clearly observed visually by placing concentrated QD colloids, with or without added biradicals, into a freezer at –40 °C. Importantly, due to the small size of the QDs (<10 nm), the voids within the aggregates are too small to allow easy access for the relatively large polarizing molecules, and are mainly filled by the 1.5-2.5 nm-long surface ligands of QDs.

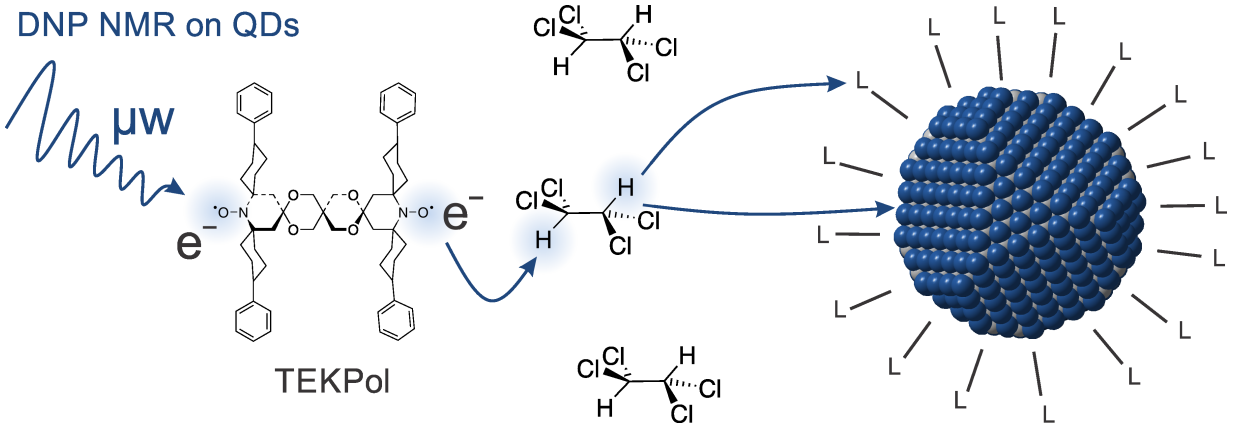

Figure 1. Schematics of the DNP surface enhanced NMR experiment for colloidal QDs. By irradiating the sample with monochromatic microwaves (from a gyrotron source, here 263 or 395 GHz, depending upon magnetic field of the NMR spectrometer), the polarization of the unpaired electron spins of the biradical is transferred to the protons of the solvent and then relayed to the protons of the ligand by spin diffusion. CP is then used to transfer DNP enhanced ^{1}H polarization to the nuclei of interest in the capping ligand layer or to the hetero-nuclei of the QD surface or QD core. Alternative pathways, omitted for clarity, are also possible, such as direct polarization transfer from the biradical to the protons of the ligand. The depth of excitation in the QD depends on the nuclei, and the CP contact time (for details of the pulse sequences used see Figure S1), allowing either signal from preferentially the uppermost surface or excitation into the subsurface layers, as discussed in the main text. L stands for organic and/or inorganic capping ligands such as oleate, myristate, oleylamine, phosphonate, sulfide, selenide *etc*. A 3 nm zinc-blende CdSe QD is shown as a model QD. 1,1,2,2-tetrachloroethane (TCE) is a known suitable DNP polarizing medium and TEKPol is a state of the art DNP polarizing agent.[32, 33]

To solve this problem, here we introduce meso-SiO_2 (3-250 nm pore sizes) as a host matrix. The meso-SiO_2 is impregnated with a solution containing both the QDs and the biradicals, thereby maintaining homogeneity of the QD-biradical mixtures in an environment similar to the native chemical environment of colloidal QDs. Inexpensive, commercially available samples of non-functionalized meso-SiO_2 were used throughout this study. Importantly, the meso-SiO_2 is highly porous (71% porous volume for MSU-H with 7-nm pore size), meaning that the dilution factor is no higher than 1.5 (close to experimentally observed, as discussed below). Furthermore, sequential filling of the pores of meso-SiO_2 first with QDs and then with polarizing agent allows, for instance, study of highly-charged inorganic-capped QDs with hydrophobic biradicals and vice-versa.

Myristate-capped InP QDs

Our initial DNP surface enhanced NMR experiments on QDs focused on myristate-capped InP QDs since ^{31}P is a highly receptive NMR nucleus, enabling the rapid optimization of sample preparation protocols. Owing to the presence of organic or inorganic capping ligand on their surfaces, 3-10 nm QDs form thermodynamically stable colloidal solutions at ambient temperatures (Figure 2a). For DNP NMR, the sample is usually loaded into a rotor at RT, and then transferred to the pre-cooled DNP NMR probe where it is quickly frozen upon cooling to 100 K. In numerous attempts to obtain DNP surface enhanced NMR spectra of QDs simply by adding biradical solutions to concentrated QD colloids we usually observed rather small DNP enhancement factors ($\varepsilon < 5$) for InP QDs (Figure 2b, d) and no enhancement for all other QD samples; in all cases due to aggregation and phase separation of QDs. On the contrary, as shown in Figure 2e, when the same colloidal solution is impregnated into commercial powders of meso-SiO_2, high DNP enhancement factors of up to 80 can be obtained. Overall, with the QD

colloid/biradical/meso-SiO_2 system an absolute QD signal enhancement by a factor of 51 is obtained by comparison to rotor filled with frozen QD colloid only, clearly outweighing the diluting effect of the added meso-SiO_2 material and possible effects from the faster relaxation due to proximity of paramagnetic biradical (Figure 2c, e and Figure S2, including detailed comparison of enhancements for various sample formulations).

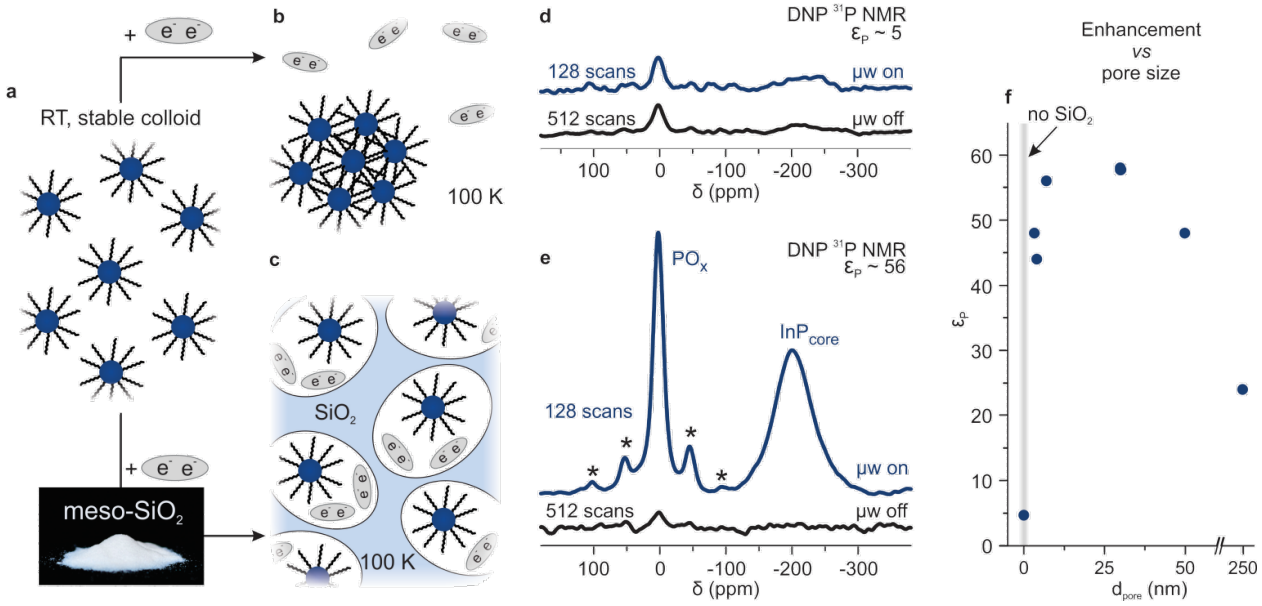

Figure 2. The effect of a meso-SiO_2 matrix on the success of DNP surface enhanced NMR experiments on colloidal myristate-capped 3 nm InP QDs. (**a**) At RT, colloidal solution of organic-ligand capped QDs is fully thermodynamically stable, often up to concentrations of 30 wt% in tetrachloroethane. This solution is then mixed with the biradical polarizing agent TEKPol, retaining colloidal stability. (**b**) In the absence of meso-SiO_2, cooling to the measurement temperature of 100 K induces aggregation of QDs and phase separation from biradicals; an effect that is easily reversed upon warming the sample after withdrawal from the cooled DNP NMR probe and which thus often goes unnoticed. (**c**) The pores of meso-SiO_2 can fully (smaller pores) or partially (large pores) limit the aggregation. Consequently, (**d**) no or very low DNP enhancements are obtained in the absence of meso-SiO_2, while, (**e**) reproducibly high enhancement factors of between 60-80 are obtained for surface PO_x signal with meso-SiO_2. In (**e**) spinning sidebands are marked by asterisks. Figure (**f**) shows the DNP enhancements obtained for InP QD-TEKPol-TCE solutions with varying pore size of the meso-SiO_2. All experiments used 1-4 mg of InP QDs per sample.

^{31}P DNP NMR spectra of 3 nm InP QDs clearly illustrate the high enhancements for signals at 0-10 ppm, assigned to surface PO_x species.[34, 35] Furthermore, a large portion of the InP QD core is also enhanced, with a very broad peak centered at –200 ppm. The intensity of the surface and core QD NMR signals depend on the contact time set in the CP pulse sequence (Figure S3), consistent with previous conventional solid-state NMR experiments on InP QDs.[35] As expected, conventional single-pulse MAS NMR spectra taken from dried powders of same InP QDs mainly show signals from the QD core (Figure S4), highlighting the utility of DNP for obtaining surface-selective information.

We then evaluated the effect of pore size of meso-SiO_2 on the DNP enhancement of the QDs, as presented for the PO_x-signal from myristate-capped InP QDs in Figure 2f. First we should note that each meso-SiO_2 sample has a distribution of pore sizes, around the one indicated as a nominal mean pore size. Thus, the 3.3 nm pore meso-SiO_2 with the smallest pore size, has in fact a relatively broad pore size distribution in the 1-8 nm range, and therefore can uptake large quantities of 3-4 nm QDs. The average population of QDs in meso-pores can vary from less than one-per-pore to as high as 20 QDs-per-pore (*i.e.* by placing a 300 mg/mL dispersion of the smallest 3 nm InP QDs, with a 2 nm-thick ligand shell, into 50 nm large spherical pores). Even if aggregation occurs in the latter case, the single aggregate size is still small enough to expose nearly all QDs to the effects of the biradical polarizing agent. A noticeable decrease in the enhancement factors can be found for all studied QDs only at extremely large pore sizes, above 100 nm, that allow aggregates sufficiently large to exclude a substantial fraction from the biradical. In control experiments without meso-SiO_2 DNP enhancements of 5 are obtained. Another beneficial effect is the inhibition of solvent crystallization in meso-SiO_2. DNP experiments typically require glass forming solvents which prevent aggregation of radicals upon

freezing.[19] Therefore, the use of meso-SiO_2 as a host for DNP experiments has the added benefit that it could allow for a broader range of solvents to be used.

CdSe QDs. After two decades of research, CdSe QDs have become a canonical QD material in academic research, and the first QD product commercialized for consumer electronics (Sony's LCD TV displays, 2013). Importantly, CdSe QDs can be deliberately obtained in two polymorphs - zinc-blende (ZB, cubic) or wurzite (WZ, hexagonal). CdSe QD surface chemistry has received a great deal of attention in recent years.[5, 12, 36, 37] The current consensus is that non-oxidized carboxylate-capped ZB-CdSe QDs (and likely WZ-CdSe QDs) comprise a CdSe core and a labile layer of surface Cd-atoms bound to carboxylate or other X-type anionic ligands, e.g. a $CdSe_{core}(CdX_2)_{shell}$ model, and therefore they are Cd-rich as a whole.[36, 38] Similar conclusions were drawn for Pb-chalcogenide QDs.[36, 39] Inspired by the ability to differentiate core and surface ^{31}P NMR signals in the InP QDs, we turned to oleate-capped ZB-CdSe QDs, containing two NMR-accessible elements ($^{111/113}Cd$ and ^{77}Se), seeking to directly probe the prevailing $CdSe_{core}(CdX_2)_{shell}$ model. With DNP surface enhanced NMR we observed a signal at –20 ppm from the QD core and a strong signal from Cd surface species at -317 ppm (Figure 3a). Both core and surface Cd signals exhibit an inhomogeneous line broadening of approximately 4000 Hz, which is considerably larger than that of bulk CdSe,[7] and likely arises from positional variations in electronic environments when moving from the surface to the core.[13, 35, 40] The NMR signal of the surface Cd atoms gives rise to an extensive manifold of spinning sidebands, which reflects a substantial chemical shift anisotropy of *ca*. 416 ppm and the lower symmetry about the surface Cd atoms. On the other hand the Cd core signal shows fewer sidebands, consistent with the more symmetric environment expected in the core. In agreement with our assignments, control single-pulse MAS NMR experiments only show signals from the ZB-CdSe QD core at -83 ppm (Figure S5). Previous direct excitation ^{113}Cd MAS NMR experiments did not study ZB-CdSe QDs, but

found ^{113}Cd chemical shifts of –96 ppm in bulk WZ-CdSe,[41] –65 ppm in WZ-CdSe QDs,[7] and –46 ppm for nearly ZB-like 2 nm CdSe nanoclusters[14] (all values are converted to a chemical shift scale with the chemical shift of Me_2Cd set to 0 ppm).

^{77}Se DNP surface enhanced NMR was also carried out for both ZB- and WZ-polymorphs, showing close chemical shifts of –579 ppm and –654 ppm (Figure 3b) and –556 ppm (Figure S6), respectively. Two peaks in Figure 3b may point to the distinct contributions from the QD core (lower intensity peak) and (near) surface Se atoms, as was previously demonstrated for WZ-CdSe QDs.[14] The ^{77}Se chemical shifts obtained from DNP experiments on WZ-CdSe match the values previously reported for WZ-CdSe QDs using conventional ^{1}H-^{77}Se CPMAS. [6, 14]

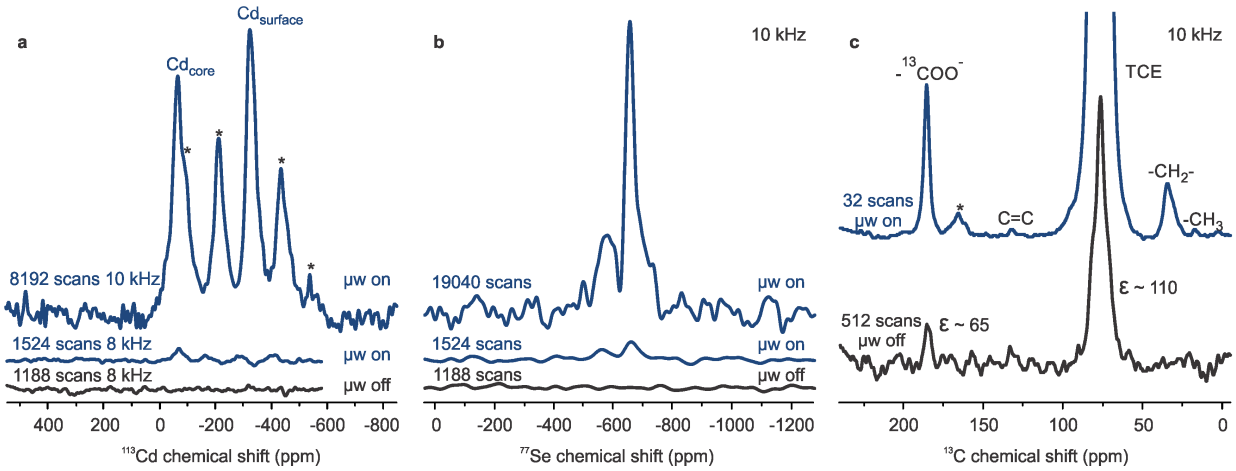

Figure 3. DNP surface enhanced NMR of oleate-capped 4nm ZB-CdSe QDs. Spectra for both the QD core (^{113}Cd and ^{77}Se, **a** nd **b**) and ligand (^{13}C, **c**) were acquired and DNP enhancements were obtained for all nuclei. The spinning side bands are marked by asterisks. Isotropic peaks and spinning sidebands were distinguished by varying the MAS frequency, Figure S7. $\delta(^{77}Se)$ is referenced to Me_2Se, $\delta(^{13}C)$ to Me_4Si, $\delta(^{113}Cd)$ to Me_2Cd (for more discussion of ^{111}Cd/^{113}Cd δ-scale in Supp. Information Table S1).

2D DNP surface enhanced hetero-nuclear correlation spectra of CdSe QDs. Figure 3c shows that using the matrix-assisted approach, DNP enhanced ^{13}C-spectra from the surface-bound oleate ligands (*e.g.* ^{13}C-1-oleate; 27% ^{13}C-labeled on the carboxylate), with clearly resolved signals

from all C-atoms, can be acquired in less than 2 minutes (32 scans). This opens the possibility to acquire ^{13}C-X hetero-nuclear 2D correlation spectra within reasonable timeframes. Partial ^{13}C-labeling of the carboxylate carbon was employed in order to help in collecting a DNP enhanced ^{13}C-^{111}Cd 2D dipolar hetero-nuclear multiple-quantum coherence (D-HMQC) correlation spectrum of oleate-capped ZB-CdSe QDs (Figure 4). Here ^{111}Cd was used rather than the more sensitive ^{113}Cd since the triple resonance probe could not be configured in ^{1}H/^{13}C/^{113}Cd mode. Such experiments yield correlations between hetero-nuclei that are close in space. The 2D spectrum (obtained overnight) shows clear correlations between carboxylate and Cd atoms at the QD surface, providing direct evidence for the $CdSe_{core}(CdX_2)_{shell}$ model, inferred previously rather indirectly from observing the ligand absorption/displacement dynamics with ^{1}H NMR.[36] Based on the signal-to-noise ratios of on/off ^{13}C-spectra, the acquisition time of non-DNP-enhanced 2D spectra would be prohibitively long, taking more than 1000 days.

Sequential filling method of meso-SiO_2 for inorganic-capped and air-sensitive QDs. In the studies presented thus far, one-step filling of meso-SiO_2 with a QD-biradical mixture was sufficient to prevent phase separation. Furthermore, common long-chain ligand-capped QDs enjoy full compatibility and miscibility with apolar solvent-biradical mixtures previously optimized for DNP. Negative consequences were encountered when attempting the same approach for highly polar, charge-stabilized QDs, such as those capped with S^{2-} and Se^{2-} ions as inorganic ligands (in the form of K_2S and K_2Se). Such inorganic capping ligands are of strategic importance for integration of QDs into (opto)electronic devices due to the high charge carrier mobility they impart into QD solids.[42, 43]

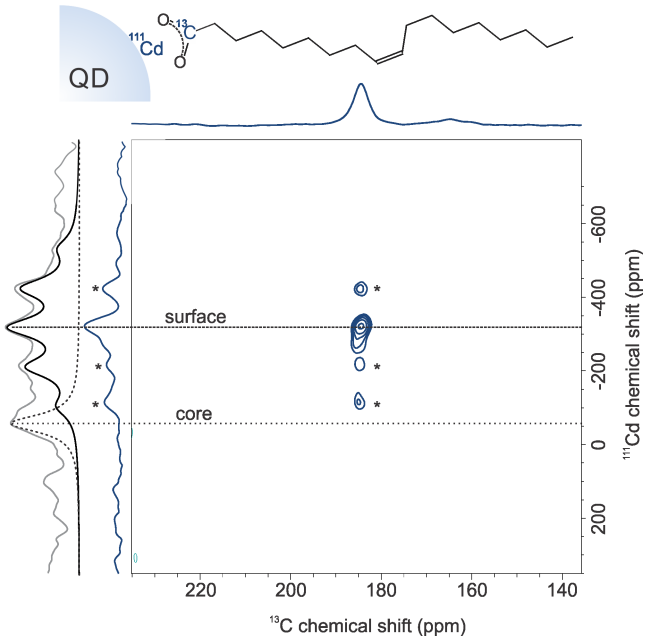

Figure 4. DNP enhanced D-HMQC spectrum correlating ^{13}C-1-oleate ligands and ^{111}Cd of ZB-CdSe. Projections of the 2D spectrum are shown in dark blue. A DNP NMR ^{111}Cd CPMAS spectrum acquired separately is shown in light grey. The isotropic shifts of the surface and core Cd-species identified before (Figure 3) are highlighted with dotted black curves. The spinning sidebands are marked by asterisks. It is apparent that the Cd-species with signal at -317 ppm is directly binding to oleic acid. No correlation between the ^{111}Cd of the QD core (-20 ppm) and ^{13}C nuclei of the ligand was observed for the recoupling time used (3 ms). Here ^{111}Cd was used rather than the more sensitive ^{113}Cd since the triple resonance probe could not be configured in ^{1}H/^{13}C/^{113}Cd mode. First order rotary resonance recoupling (R^3) was employed.

There are much fewer polar solvent-biradical mixtures which simultaneously solubilize charge-stabilized QDs and allow for efficient DNP enhancements. The only working example we identified so far is AMUPol in DMSO-d^6/H_2O/D_2O, which is suitable for studying chemically robust materials such as sulfide capped Sn/SnO_x nanocrystals.[22] Water in this mixture is required for efficient polarization transfer, but promotes hydrolysis and oxidation of sensitive QD materials. To circumvent these problems, a facile and versatile two-step method for filling the meso-SiO_2 matrix is presented in Figure 5. This method eliminates a tedious search for suitable compatible QD-solvent-radical combinations. First, impregnation of the meso-SiO_2 was done

with a QD dispersion in any given type of solvent, polar or apolar, followed by the evaporation of the solvent to deposit the QDs in the meso-SiO_2. Second, the meso-SiO_2 filled with QDs was then impregnated with any other given (polar or apolar) biradical-solvent mixture. Hence apolar solvent-biradical combinations can be used for enhancing NMR signals of highly polar inorganic-capped QDs, and vice-versa. In the first case study, highly oxygen and moisture-sensitive selenide (Se^{2-}) capped CdSe QDs, prepared from oleate-capped QDs via a ligand-exchange reaction,[28] were deposited into meso-SiO_2 from formamide solution. Subsequent ^{77}Se DNP NMR with the TEKPol-TCE polarization mixture yields a spectrum with higher signal-to-noise ratio (Figure 5a, 3000 scans) than was obtained for carboxylate-capped CdSe NCs (Figure 3b). The ^{77}Se spectrum of CdSe-Se^{2-} QDs is, however, asymmetrically broader (see direct comparison in Figure S8), presumably due to contribution from the surface-bound Se^{2-} with a chemical shift only subtly different to the core Se nuclei. This conclusion is supported by the control experiments with unbound Se^{2-}, where the ^{77}Se chemical shifts of frozen solutions and powders of K_2Se were much further separated (by several hundred ppm, Figure S8).

More chemically robust sulfide (S^{2-}) inorganic-capped InP QDs are compatible with an AMUPol-DMSO-d^6/H_2O/D_2O polarizing mixture, allowing direct comparison between one-step and two-step filling methods. Similar DNP enhancement factors were obtained in both cases (Figure 5b and c), yet with a noticeable difference in the obtained ^{31}P NMR spectra. The ^{31}P CPMAS NMR spectrum from the two-step, water-free deposition features an additional peak (marked with an arrow in Figure 5c). Although the chemical identity of this signal is not fully clear, we can speculate that they are due to PO_xS_y surface species, which are otherwise fully oxidized and/or hydrolyzed in a water-based polarizing mixture.

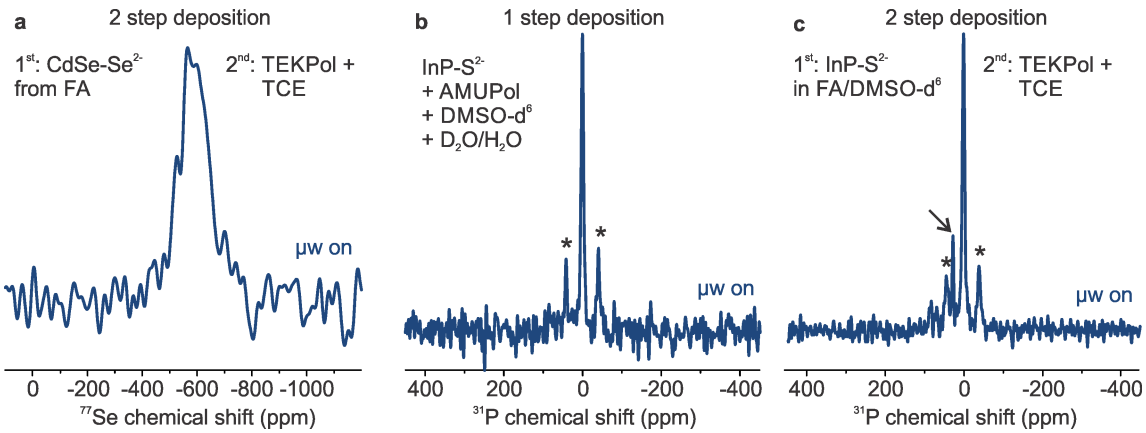

Figure 5. DNP surface enhanced NMR on air-sensitive and inorganic-capped QDs using sequential filling of meso-SiO_2 (two-step method). CdSe-Se^{2-} QDs are highly oxygen and moisture sensitive and could be studied only with two-step deposition method (**a**). InP-S^{2-} QDs have been deposited into silica pores by one (**b**) and two-step (**c**) procedures. The two-step procedure does not involve any water during preparation and yields an additional peak in the spectrum (indicated by an arrow), attributed to PO_xS_y species, absent in (**b**) due to full conversion into PO_x species. The spinning sidebands are marked by asterisks.

Other tested systems, concluding remarks and outlook.

So far precipitation of QDs to form powdered samples had remained the only practical option for solid-state NMR studies on QDs. Precipitation may change the chemical identity of the surface QD atoms and/or surface ligands. In this study, we have shown that meso-SiO_2-assisted DNP experiments allow for using colloidal dispersions of QDs directly for solid-state NMR spectroscopy to study QDs in an environment more similar to a dispersion. Owing to efficient proton DNP enhancements (ε_H = 40-80), absolute signals obtained with small sample amounts (1-4 mg of QDs per sample throughout this study) are always much greater than conventional MAS NMR signals from a rotor densely packed with large quantities of QDs (up to 100-200 mg). In fact, there are clear physical and hardware limits to scaling the MAS NMR signal by using larger sample quantities and larger rotors. Without DNP enhancement, acquisition of 1D CPMAS

spectra from 1-2 mg of QDs would take months or even years. The matrix–assisted method enables acquisition of 2D spectra between hetero-nuclei in reasonable timeframes (hours instead of years) and allows a whole new plethora of studies to be carried out, such as directly probing metal-ligand binding at the QD surface (as shown here for Cd-oleate at the CdSe surface), and possibly intra-ligand and intra-QD local chemical structure. With a two-step sequential filling method, problems such as air and moisture sensitivity, solvent incompatibility and low solubility can be easily circumvented. With the advent of commercial DNP NMR spectrometers, and the active development of suitable biradical polarization transfer agents,[32, 44] DNP enhanced NMR spectroscopy holds great promise to address various research problems in contemporary nanomaterials research. Meso-SiO_2 of appropriate pore size is also likely to be of great help for ensuring homogeneous DNP excitation of many other important analytes such as polymers, biomolecules, colloids, and coordination compounds, yet with minimal dilution effect.

Specific to the chemistry of QDs, DNP surface enhanced NMR yields signatures from the QD core, QD surface, and surface-bound ligands. For CdSe QDs as a case study, we were able for the first time to clearly distinguish Cd atoms from the QD core and QD surface, thanks to the tunable surface-selectivity of DNP.. Hence strong evidence is obtained here in support of a $CdSe_{core}(CdX_2)_{shell}$ (X=oleate ligand) morphology of these QDs. Correspondingly, ^{77}Se spectra point to the gradient of chemical shifts within the QD core, rather than new surface species. Furthermore, large DNP enhancements permitted fast acquisition of ^{111}Cd-^{13}C 2D-correlation spectra within the surface Cd-carboxylate layer, directly determining ligand binding to the CdSe QD surface. Future studies will expand such analysis to shape and composition engineered CdSe nanostructures such as atomically flat CdSe nanoplatelets[45] or highly-luminescent core-shell $CdSe/Cd_{1-x}Zn_xS$ QDs (x=0-1).[46, 47] Besides two detailed case studies – InP and CdSe QDs – we were also able to record DNP enhanced spectra for a variety of other important QD core materials

in a short survey study (DNP enhanced nuclei in parentheses, see Figure S9): PbSe (^{77}Se), CdTe (^{125}Te), and PbTe (^{125}Te). ^{125}Te DNP enhanced spectra, as an example, illustrate large difference in stability with respect to oxidation of CdTe and PbTe QDs. We observe that PbTe QDs comprise exclusively Te-oxide species at their surfaces, even when freshly prepared and handled air-free, while CdTe QDs remain un-oxidized upon long storage in air. These preliminary results pave the way towards new atomistic insights into the chemistry of these QDs in future studies. In another trial, we deposited nanocrystalline $CsPbBr_3$, perovskite-type highly luminescent semiconductors,[48] into pores of meso-SiO_2 and recorded DNP enhanced spectra of ^{133}Cs (Figure S10), for the first time for this nucleus to the best of our knowledge. This result highlights the utility and future prospects of DNP also for nanomaterials containing quadrupolar nuclei.

Acknowledgements M.K. acknowledges financial support from the European Union through the FP7 (ERC Starting Grant NANOSOLID, GA No. 306733) and L.E. acknowledges support from ERC Advanced Grant No. 320860. René Verel and Maxence Valla are acknowledged for their help at the NMR facility at ETH Zurich. Davisil Silica matrices with ≥50nm pore sizes were gifts of GRACE. Georgian Nedelcu is acknowledged for providing InP QDs, Tanja Zünd for CdTe QDs, Maria Ibáñez Sabate for PbTe QDs, David Trummer for $CsPbBr_3$ nanostructures, and Indre Thiel for supplying meso-SiO_2 with 3.3 nm pore size.

Competing financial interests: The authors declare no competing financial interest.

Supporting information. Materials, Methods, Supporting Figures S1-S10 and Table S1 and additional explanations are available free of charge via the Internet at http://pubs.acs.org/.

Author information

L.P. synthesized W-CdSe, ZB-CdSe, and PbSe QDs, prepared inorganic-capped QDs, and formulated all samples for DNP NMR; L.P., A.J.R. and T.C.O. carried out DNP NMR measurements; L.P., A.J.R. and T.C.O. analysed DNP NMR data; M.K., C.C. and L.E. conceived and supervised the project. The manuscript was prepared through the contribution of all authors.

Corresponding author:

mvkovalenko@ethz.ch; ccoperet@ethz.ch; lyndon.emsley@epfl.ch

References

1. Chen, O.; Riedemann, L.; Etoc, F.; Herrmann, H.; Coppey, M.; Barch, M.; Farrar, C. T.; Zhao, J.; Bruns, O. T.; Wei, H.; Guo, P.; Cui, J.; Jensen, R.; Chen, Y.; Harris, D. K.; Cordero, J. M.; Wang, Z.; Jasanoff, A.; Fukumura, D.; Reimer, R.; Dahan, M.; Jain, R. K.; Bawendi, M. G. *Nat. Commun.* **2014**, 5:5093 doi: 10.1038/ncomms6093.
2. Medintz, I. L.; Stewart, M. H.; Trammell, S. A.; Susumu, K.; Delehanty, J. B.; Mei, B. C.; Melinger, J. S.; Blanco-Canosa, J. B.; Dawson, P. E.; Mattoussi, H. *Nat. Mater.* **2010,** 9, 676-684.
3. Talapin, D. V.; Lee, J.-S.; Kovalenko, M. V.; Shevchenko, E. V. *Chem. Rev.* **2010,** 110, 389-458.
4. Kim, D. K.; Lai, Y.; Diroll, B. T.; Murray, C. B.; Kagan, C. R. *Nat. Commun.* **2012**, 3:1216 doi: 10.1038/ncomms2218.
5. Owen, J. *Science* **2015,** 347, 615-616.
6. Lovingood, D. D.; Achey, R.; Paravastu, A. K.; Strouse, G. F. *J. Am. Chem. Soc.* **2010,** 132, 3344-3354.
7. Ratcliffe, C. I.; Yu, K.; Ripmeester, J. A.; Badruz Zaman, M.; Badarau, C.; Singh, S. *Phys. Chem. Chem. Phys.* **2006,** 8, 3510-3519.
8. Abraham, A.; Mihaliuk, E.; Kumar, B.; Legleiter, J.; Gullion, T. *J. Phys. Chem. C* **2010,** 114, 18109-18114.
9. Yesinowski, J. P., Solid-state NMR of inorganic semiconductors. In *Solid state NMR*, Chan, J. C. C., Ed. 2012; Vol. 306, pp 229-312.
10. Sachleben, J. R.; Colvin, V.; Emsley, L.; Wooten, E. W.; Alivisatos, A. P. *J. Phys. Chem. B* **1998,** 102, 10117-10128.
11. Sachleben, J. R.; Wooten, E. W.; Emsley, L.; Pines, A.; Colvin, V. L.; Alivisatos, A. P. *Chem. Phys. Lett.* **1992,** 198, 431-436.

12. Hens, Z.; Martins, J. C. *Chem. Mat.* **2013,** 25, 1211-1221.
13. Cadars, S.; Smith, B. J.; Epping, J. D.; Acharya, S.; Belman, N.; Golan, Y.; Chmelka, B. F. *Phys. Rev. Lett.* **2009,** 103, 136802.
14. Berrettini, M. G.; Braun, G.; Hu, J. G.; Strouse, G. F. *J. Am. Chem. Soc.* **2004,** 126, 7063-7070.
15. Maly, T.; Debelouchina, G. T.; Bajaj, V. S.; Hu, K.-N.; Joo, C.-G.; Mak-Jurkauskas, M. L.; Sirigiri, J. R.; van der Wel, P. C. A.; Herzfeld, J.; Temkin, R. J.; Griffin, R. G. *J. Chem. Phys.* **2008,** 128, 052211.
16. Ni, Q. Z.; Daviso, E.; Can, T. V.; Markhasin, E.; Jawla, S. K.; Swager, T. M.; Temkin, R. J.; Herzfeld, J.; Griffin, R. G. *Acc. Chem. Res.* **2013,** 46, 1933-1941.
17. Lesage, A.; Lelli, M.; Gajan, D.; Caporini, M. A.; Vitzthum, V.; Miéville, P.; Alauzun, J.; Roussey, A.; Thieuleux, C.; Mehdi, A.; Bodenhausen, G.; Coperet, C.; Emsley, L. *J. Am. Chem. Soc.* **2010,** 132, 15459-15461.
18. Lelli, M.; Gajan, D.; Lesage, A.; Caporini, M. A.; Vitzthum, V.; Mieville, P.; Heroguel, F.; Rascon, F.; Roussey, A.; Thieuleux, C.; Boualleg, M.; Veyre, L.; Bodenhausen, G.; Coperet, C.; Emsley, L. *J. Am. Chem. Soc.* **2011,** 133, 2104-2107.
19. Rossini, A. J.; Zagdoun, A.; Lelli, M.; Lesage, A.; Copéret, C.; Emsley, L. *Acc. Chem. Res.* **2013,** 46, 1942-1951.
20. Sangodkar, R. P.; Smith, B. J.; Gajan, D.; Rossini, A. J.; Roberts, L. R.; Funkhouser, G. P.; Lesage, A.; Emsley, L.; Chmelka, B. F. *J. Am. Chem. Soc.* **2015,** 137, 8096-8112.
21. Perras, F. A.; Kobayashi, T.; Pruski, M. *J. Am. Chem. Soc.* **2015,** 137, 8336-8339.
22. Protesescu, L.; Rossini, A. J.; Kriegner, D.; Valla, M.; de Kergommeaux, A.; Walter, M.; Kravchyk, K. V.; Nachtegaal, M.; Stangl, J.; Malaman, B.; Reiss, P.; Lesage, A.; Emsley, L.; Copéret, C.; Kovalenko, M. V. *ACS Nano* **2014,** 8, 2639-2648.
23. Corzilius, B.; Michaelis, V. K.; Penzel, S. A.; Ravera, E.; Smith, A. A.; Luchinat, C.; Griffin, R. G. *J. Am. Chem. Soc.* **2014,** 136, 11716-11727.
24. Wolf, P.; Valla, M.; Rossini, A. J.; Comas-Vives, A.; Núñez-Zarur, F.; Malaman, B.; Lesage, A.; Emsley, L.; Copéret, C.; Hermans, I. *Angew. Chem. Int. Ed.* **2014,** 53, 10179-10183.
25. Akbey, Ü.; Altin, B.; Linden, A.; Özçelik, S.; Gradzielski, M.; Oschkinat, H. *Phys. Chem. Chem. Phys.* **2013,** 15, 20706-20716.
26. Lafon, O.; Thankamony, A. S. L.; Rosay, M.; Aussenac, F.; Lu, X.; Trebosc, J.; Bout-Roumazeilles, V.; Vezin, H.; Amoureux, J.-P. *Chem. Commun.* **2013,** 49, 2864-2866.
27. Zagdoun, A.; Rossini, A. J.; Gajan, D.; Bourdolle, A.; Ouari, O.; Rosay, M.; Maas, W. E.; Tordo, P.; Lelli, M.; Emsley, L.; Lesage, A.; Coperet, C. *Chem. Commun.* **2012,** 48, 654-656.
28. Nag, A.; Kovalenko, M. V.; Lee, J.-S.; Liu, W.; Spokoyny, B.; Talapin, D. V. *J. Am. Chem. Soc.* **2011,** 133, 10612-10620.
29. Rosay, M.; Tometich, L.; Pawsey, S.; Bader, R.; Schauwecker, R.; Blank, M.; Borchard, P. M.; Cauffman, S. R.; Felch, K. L.; Weber, R. T.; Temkin, R. J.; Griffin, R. G.; Maas, W. E. *Phys. Chem. Chem. Phys.* **2010,** 12, 5850-5860.
30. Pines, A.; Gibby, M.; Waugh, J. *J. Chem. Phys.* **1973,** 59, 569-590.
31. Hall, D. A.; Maus, D. C.; Gerfen, G. J.; Inati, S. J.; Becerra, L. R.; Dahlquist, F. W.; Griffin, R. G. *Science* **1997,** 276, 930-932.
32. Zagdoun, A.; Casano, G.; Ouari, O.; Schwaerzwalder, M.; Rossini, A. J.; Aussenac, F.; Yulikov, M.; Jeschke, G.; Coperet, C.; Lesage, A.; Tordo, P.; Emsley, L. *J. Am. Chem. Soc.* **2013,** 135, 12790-12797.
33. Matsuki, Y.; Maly, T.; Ouari, O.; Karoui, H.; Le Moigne, F.; Rizzato, E.; Lyubenova, S.; Herzfeld, J.; Prisner, T.; Tordo, P.; Griffin, R. G. *Angew. Chem. Int. Ed.* **2009,** 48, 4996-5000.
34. Cros-Gagneux, A.; Delpech, F.; Nayral, C.; Cornejo, A.; Coppel, Y.; Chaudret, B. *J. Am. Chem. Soc.* **2010,** 132, 18147-18157.
35. Tomaselli, M.; Yarger, J. L.; Bruchez, M.; Havlin, R. H.; deGraw, D.; Pines, A.; Alivisatos, A. P. *J. Chem. Phys.* **1999,** 110, 8861-8864.

36. Anderson, N. C.; Hendricks, M. P.; Choi, J. J.; Owen, J. S. *J. Am. Chem. Soc.* **2013,** 135, 18536-18548.
37. Kovalenko, M. V.; Manna, L.; Cabot, A.; Hens, Z.; Talapin, D. V.; Kagan, C. R.; Klimov, V. I.; Rogach, A. L.; Reiss, P.; Milliron, D. J.; Guyot-Sionnnest, P.; Konstantatos, G.; Parak, W. J.; Hyeon, T.; Korgel, B. A.; Murray, C. B.; Heiss, W. *ACS Nano* **2015,** 9, 1012-1057.
38. Fritzinger, B.; Capek, R. K.; Lambert, K.; Martins, J. C.; Hens, Z. *J. Am. Chem. Soc.* **2010,** 132, 10195-10201.
39. Zherebetskyy, D.; Scheele, M.; Zhang, Y.; Bronstein, N.; Thompson, C.; Britt, D.; Salmeron, M.; Alivisatos, P.; Wang, L.-W. *Science* **2014,** 344, 1380-1384.
40. Thayer, A. M.; Steigerwald, M. L.; Duncan, T. M.; Douglass, D. C. *Phys. Rev. Lett.* **1988,** 60, 2673-2676.
41. Nolle, A. *Z. Naturforsch. A* **1978,** 33 a, 6.
42. Jang, J.; Liu, W.; Son, J. S.; Talapin, D. V. *Nano Lett.* **2014,** 14, 653-662.
43. Lee, J.-S.; Kovalenko, M. V.; Huang, J.; Chung, D. S.; Talapin, D. V. *Nat. Nanotechnol.* **2011,** 6, 348-352.
44. Kiesewetter, M. K.; Corzilius, B.; Smith, A. A.; Griffin, R. G.; Swager, T. M. *J. Am. Chem. Soc.* **2012,** 134, 4537-4540.
45. Bouet, C.; Tessier, M. D.; Ithurria, S.; Mahler, B.; Nadal, B.; Dubertret, B. *Chem. Mat.* **2013,** 25, 1262-1271.
46. Dang, C.; Lee, J.; Breen, C.; Steckel, J. S.; Coe-Sullivan, S.; Nurmikko, A. *Nat. Nanotechnol.* **2012,** 7, 335-339.
47. Chen, O.; Zhao, J.; Chauhan, V. P.; Cui, J.; Wong, C.; Harris, D. K.; Wei, H.; Han, H.-S.; Fukumura, D.; Jain, R. K.; Bawendi, M. G. *Nat. Mater.* **2013,** 12, 445-451.
48. Stoumpos, C. C.; Malliakas, C. D.; Peters, J. A.; Liu, Z.; Sebastian, M.; Im, J.; Chasapis, T. C.; Wibowo, A. C.; Chung, D. Y.; Freeman, A. J.; Wessels, B. W.; Kanatzidis, M. G. *Cryst. Growth Des.* **2013,** 13, 2722-2727.

Supportiung Information for

The Structure of Colloidal Quantum Dots from Dynamic Nuclear Polarization Surface Enhanced NMR Spectroscopy

Laura Piveteau,[† ‡] Ta-Chung Ong,[†] Aaron J. Rossini,[§] Lyndon Emsley,[§] Christophe Copéret[* †] and Maksym V. Kovalenko[* † ‡]*

*Email: mvkovalenko@ethz.ch; ccoperet@ethz.ch; lyndon.emsley@epfl.ch

[†] Department of Chemistry and Applied Biosciences, ETH Zürich, Vladimir Prelog Weg 1-5, CH-8093, Switzerland

[‡]Empa-Swiss Federal Laboratories for Materials Science and Technology, Dübendorf, Überlandstrasse 129, CH-8600, Switzerland

[§]Institut des Sciences et Ingénierie Chimiques, Ecole Polytechnique Fédérale de Lausanne (EPFL), 1015 Lausanne, Switzerland

CONTENT

I. Materials

Chemicals and solvents. Acetone (anhydrous, Fischer Scientific), acetonitrile (MeCN, ≥99.9%, Aldrich), bis[bis(trimethylsilyl)-amino] tin(II) ($Sn[N(TMS)_2]_2$, Aldrich), bis(trimethylsilyl)sulfide ($(TMS)_2S$, Aldrich), cesium bromide (CsBr, Merck), chloroform ($CHCl_3$, anhydrous, 99+%, Aldrich), cadmium oxide (CdO, 99.99+%, Aldrich), deuterated water (D_2O, 99.9atom%, Cambridge Isotope Lab), dimethylsulfoxide deuterated (DMSO-d^6, 99,9atom%, Cambridge Isotope Lab), dipotassium sulfide (K_2S, 95%, STREM), ethanol (EtOH, dried, max. H_2O 0.01%, Merck), formamide (FA, 99+%, Aldrich), hexane (≥95%, Aldrich), hydrobromic acid (HBr, Aldrich), indium (III) acetate ($In(Ac)_3$, 99.99%, Aldrich), isopropanol (IPA, ≥99.5%, Aldrich), lead acetate trihydrate ($Pb(OAc)_2 \cdot 3H_2O$, ≥99.99%, Aldrich), lead bromide ($PbBr_2$, 99.999%, abcr), lead chloride ($PbCl_2$, 99.999%, abcr), methanol (MeOH, ≥99.9%, Aldrich), ethanol (EtOH, ≥99.8%, Aldrich), myristic acid (MA, ≥99%, Aldrich), N,N-dimethylformamide (DMF, Aldrich), 1-octadecene (ODE, 90%, Aldrich), octadecylphosphonic acid (ODPA, 97%, PCI Synthesis), 1-octylamine (99%, Aldrich), oleic acid (OA, 90%, Aldrich), oleylamine (OLA, tech. 70%, Aldrich), selenium (Se, 100 mesh, 99.99%, Aldrich), selenium dioxide (SeO_2, 99.999%, STREM), tellurium shots (Te, 99.999%, Aldrich), tetrachloroethane (TCE, ≥98%, Aldrich or 98.5% ACROS), tetrachloroethylene (anhydrous, >99%, Aldrich), toluene (≥99.9%, Aldrich), tributyl phosphine (TBP, Aldrich), trioctylphophine (TOP, 97%, STREM), trioctylphosphine oxide (TOPO, 99%, Aldrich), tris(trimethylsilyl)phosphine ($P(TMS)_3$, 0.6 mM, 98%, Strem), water (H_2O, Merck), dipotassium selenide (K_2Se) was synthesized as reported by McCarthy *et al*.[1]

Biradical polarizing agents. TEKPol[2] and AMUPol[3] were provided by Dr. Olivier Ouari, Dr. Gilles Casano and Prof. Dr. Paul Tordo (Aix-Marseille Université).

Meso-SiO_2 matrices. Mesoporous silica (3.3 nm pore size, provided by Indre Thiel from Copéret group based on synthesis reported elsewhere[4, 5]), silica (200 nm particles, 4 nm pore size, 200 nm particle size Aldrich), hexagonal mesostructured silica (MSU-H, 7 nm pore size, Aldrich), 15 nm silica (Davisil Grade 643, Aldrich), 30 nm silica gel (spherical shapes, AlfaAesar), 50 nm silica (SP 541-10309, ID 7765, GRACE), 250 nm silica (SP 541-10309, GRACE).

II. Syntheses of colloidal QDs

All syntheses were conducted under air-free conditions using Schlenk technique and argon-filled glove boxes (O_2 and H_2O levels < 1 ppm).

3 nm myristate-capped InP QDs were synthesized using a modified method from Ref.[6] 0.35 g $In(Ac)_3$ (1.2 mmol), 1.14 g MA (5 mmol) and 20 mL ODE were loaded into a 3-neck flask and dried under vacuum for 75 minutes at 125 °C to form indium myristate. The reaction mixture was heated up to 188 °C under N_2 flow. $P(TMS)_3$ (0.6 mM) and dried 2.4 mL OLA (7.2 mmol) in 3 mL ODE were mixed in a glove box, loaded into a syringe and swiftly injected into the hot reaction mixture. Immediately after injection, the reaction temperature was decreased down to 178 °C and kept at this value for 1 hour to allow the growing of InP QDs. The QDs were purified by addition of hexane to the reaction mixture and precipitated with a mixture of MeOH:IPA (1:1). The precipitate was separated from solvent by centrifugation and redispersed in hexane. The washing process was repeated four times. Purified InP QDs were redispersed and stored in hexane.

3.5 nm oleate-capped ZB-CdSe QDs were prepared according to a slightly modified synthesis procedure of Chen *et al.*[7] 83 mg CdO (0.65 mmol), 25 mL ODE and 1.2 mL OA (3.4 mmol) were dried under vacuum for 1 h at 100 °C. Heating up to 240 °C under nitrogen flow lead to complete dissolution of CdO forming transparent colorless solution. The cadmium oleate solution was let cooling down to room temperature and then 75 mg SeO_2 (0.68 mmol) was added to the reaction flask. Under vigorous stirring the suspension was quickly heated up to 230 °C. The reaction was stopped after 10 seconds of growing time by quickly cooling down to room temperature. Particles were washed three times with toluene/EtOH and finally dissolved in hexane.

4.5 nm oleate-capped CdTe QDs were prepared according to slightly modified synthetic procedure by Panthani *et al.*[8] 1.2 g CdO (9 mmol), 12 mL OA (34 mmol) and 16.5 mL ODE were dried for 1 hour under vacuum at 100 °C. Under nitrogen flow, the suspension was heated up to 270 °C and a transparent, colorless solution was obtained. 5 mL of 1 M Te-TBP solution was swiftly injected and the reaction mixture was let to cool down to room temperature. The CdTe QDs were washed four times with toluene/EtOH and finally redispersed in toluene.

3 nm phosphonate-capped WZ-CdSe QDs were prepared following synthetic procedure reported by Bawendi *et al.*[9] 60 mg CdO (0.467 mmol), 282 mg ODPA (0.843 mmol), and 3 g TOPO (7.798 mmol) were dried under vacuum for one hour at 150 °C. The suspension was heated up to 230 °C under nitrogen flow until all CdO was dissolved and a transparent colorless solution obtained. At 320 °C, 1 mL of TOP was added. At 360 °C, TOP-Se solution (61 mg, 0.772 mmol Se in 500 µL TOP) was swiftly injected and the heating mantle was removed. After 90 seconds the reaction mixture was quickly cooled down to room temperature. Anhydrous toluene (5 mL) was added to prevent TOPO from solidifying. QDs were washed using toluene/EtOH solvent/nonsolvent system. Small quantities of octylamine were used to facilitate purification of the QDs.

4 nm oleate-capped PbSe QDs were synthezised following synthetic procedure reported by Kovalenko *et al.*[10] 0.2 mg $PbCl_2$ (0.719 mmol) and 7 mL OLA were dried for 15 minutes under vacuum at room temperature. Suspension is quickly heated up to 135 °C under N_2 flow and 1 M TOP-Se (250 mg, 3 mmol Se in 3 mL TOP) combined with 400 µL 1 M $Sn[N(TMS)_2]_2$ solution (1 mmol $Sn[N(TMS)_2]_2$ in 1 mL

TOP) was swiftly injected. After 2 min at 120 °C, the black reaction mixture was quickly cooled down to room temperature. At 50 °C, 1.5 mL OA 1.5 mL was added to replace weakly bound OLA molecules. QDs were washed under inert atmosphere in glovebox using $CHCl_3$/EtOH as a solvent/antisolvent system.

6.5 nm oleate-capped PbTe QDs were prepared similarly to previously reported procedure of Urban et al.[11] $Pb(OAc)_2 \cdot 3H_2O$ (0.5685 g, 1.75 mmol) and OA (1.0 mL) were mixed with ODE (10 mL). This mixture was degassed at room temperature, 50 ºC, 70 ºC, 90 ºC and 110 ºC for 10 minutes each to form lead oleate. Then the solution was flushed with nitrogen, and the temperature was raised to 180 °C. At this temperature, 12 mL Te-precursor (0.25 M), prepared by dissolving tellurium shots in TOP was rapidly injected. The reaction mixture was maintained at 160-170 °C for 3 minutes and then quickly cooled down to room temperature using a water bath. PbTe QDs were thoroughly washed in inert atmosphere by multiple precipitation/redispersion steps using anhydrous acetone as a non-solvent and anhydrous tetrachloroethylene as solvent and finally redispersed in anhydrous tetrachloroethylene.

Bulk $CsPbBr_3$ was synthesized according to Stoumpos *et al.*[12] 0.9 g $PbBr_2$ (2.5 mmol) and 0.9 g CsBr (4.5 mmol) were solubilized in 0.2 g 48% aqueous HBr (2.5 mmol) and 2.5 mL H_2O. After stirring overnight at room temperature, the bright orange precipitate was separated by filtration and washed with absolute EtOH. The pure $CsPbBr_3$ obtained was dried under vacuum and stored in dry conditions.

$CsPbBr_3$ nanostructures encapsulated in meso-SiO_2. 10.5 mg meso-SiO_2 (7 nm pore size) was impregnated with 21 µL $CsPbBr_3$ solution (0.083 M in DMF), dried, and heated for 20 minutes at 150 °C under vacuum.

III. Preparation of inorganic capped QDs

Sulfide-capped InP QDs. 7.7 mg K_2S (anhydrous) was dissolved in 1.5 mL FA (dried) and mixed with 5 mg myristate-capped InP in 1.5 mL hexane. The two-phase mixture was stirred for *ca*. 2 hours until complete migration of the QDs from the apolar to the polar phase. The colorless supernatant solution was discarded and the red FA phase was washed three times with fresh hexane. The QDs were precipitated with 1.5 mL MeCN, collected by centrifugation and redispersed in FA or DMSO-d^6/H_2O (6:4 by volume).

Selenide-capped CdSe QDs. All procedures were carried out in a glovebox. 6 mg oleate-capped CdSe QDs were dispersed in 3 mL dried toluene and mixed with 3 mL dried FA containing excess of K_2Se (21 mg). Two-phase mixture was stirred for 2 hours until supernatant solution turned colorless and the FA phase dark red. Toluene phase was discarded and the polar phase was washed three times with fresh dried toluene. Colloidal solution was filtered (0.45 μm PTFE filter) and QDs were precipitated with 1.5 mL MeCN. Precipitate was collected by centrifugation and redispersed in minimal amount of dried FA (60 μL).

IV. Conventional MAS solid-state NMR

^{133}Cs and ^{31}P NMR spectra were acquired on a Bruker 11.7 T spectrometer equipped with a 2.5 mm two channel solid-state probe head and an Avance III console. Experiments were performed at room temperature using MAS spinning frequencies of 20 kHz and 2.5 mm zirconia rotors.

^{77}Se NMR spectra at 100 K were acquired on a commercial Bruker 14.1 T instrument equipped with an Avance III console and a triple and a double resonance 3.2 mm low temperature MAS probe while spinning at 10 kHz using sapphire rotors. ^{77}Se NMR spectra at room temperature were acquired on a Bruker 11.7 T spectrometer equipped with a 2.5 mm two channel solid-state probe head and an Avance III console. MAS spinning frequencies of 20 kHz and 2.5 mm zirconia rotors were used.

^{113}Cd NMR spectra were measured on a Bruker 16.4 T magnet equipped with a 4 mm two channel solid-state probe head and an Avance III console. Experiments were performed at room temperature and at low MAS spinning rates of 600 Hz.

Detailed experimental conditions such as pulse sequence, spinning frequency of the MAS, pulse length, etc. are listed below in "VI. Supplementary figures and details for displayed NMR spectra" and "VII. Details for all NMR experiments presented in main text".

Chemical shifts were referenced to 0.1 M aqueous solution of CsCl (^{133}Cs), 85% H_3PO_4 in H_2O (^{31}P), Me_2Se (^{77}Se) and Me_2Cd (^{113}Cd). Referencing of ^{77}Se and ^{113}Cd chemical shifts was performed with the less toxic secondary standards $NaSeO_3$ and $Cd(ClO_4)_2 \cdot 6H_2O$ with known chemical shifts of 1260 ppm and -641 ppm, respectively.

Table S1: For ^{111}Cd and ^{113}Cd NMR IUPAC recommends to use neat Me_2Cd as reference compound.[13] However, often less toxic inorganic reference materials are used. Table below presents the summary by Duncan of most important standards.[14]

Reference compound	Me_2Cd (ppm)	$CdCl_2$ (ppm)	$Cd(ClO_4)_2 \cdot 6H_2O$ (ppm)	0.1 M $Cd(ClO_4)_2$ (ppm)	$Cd(NO_3)_2 \cdot 4H_2O$ (ppm)
Me_2Cd	0	-435	-641	-641	-741
$CdCl_2$	435	0	-206	-206	-306
$Cd(ClO_4)_2 \cdot 6\ H_2O$	641	206	0	0	-100
0.1 M $Cd(ClO_4)_2$	641	206	0	0	-100
$Cd(NO_3)_2 \cdot 4\ H_2O$	741	306	100	100	0

V. DNP NMR

DNP NMR measurements were performed on two different machines.

At ETH Zürich, experiments were conducted on a commercial Bruker 14.1 T DNP NMR spectrometer equipped with an Avance III console and triple or double resonance 3.2 nm low temperature MAS probe. The microwave frequency of 395 GHz was generated by a Bruker gyrotron which output an approximate microwave power of 6 W.

At EPF Lausanne, a commercial Bruker 9.4 T DNP solid-state NMR spectrometer equipped with an Avance I console, a 263 GHz gyrotron microwave source and a triple resonance 3.2 mm low temperature MAS probe was employed.[15] The microwave output power was ca. 5 W.

CP transfer[16] was conducted with variable amplitude during contact time.[17] The SPINAL-64 hetero-nuclear decoupling sequence[18] with a radio frequency (rf) field of 100 kHz was used for all DNP NMR experiments. Chemical shifts were referenced to Me_4Si (^{1}H, ^{13}C), 85% H_3PO_4 in H_2O (^{31}P), Me_2Se (^{77}Se), Me_2Cd ($^{111/113}Cd$), Me_2Te (^{125}Te), 0.1 M CsCl in H_2O (^{133}Cs). Referencing of ^{77}Se, ^{113}Cd and ^{125}Te chemical shifts was performed with the less toxic secondary standards $NaSeO_3$, $Cd(ClO_4)_2 \cdot 6H_2O$ and $Te(OH)_6$ with known chemical shifts of 1260 ppm, -641 ppm and 713 ppm, respectively.

Detailed experimental conditions such as pulse sequence, spinning frequency of the MAS, pulse length, etc. are listed below in “VI. Supplementary figures and details for displayed NMR spectra” and “VII. Details for all NMR experiments presented in main text”.

VI. Supplementary figures and details for displayed NMR spectra

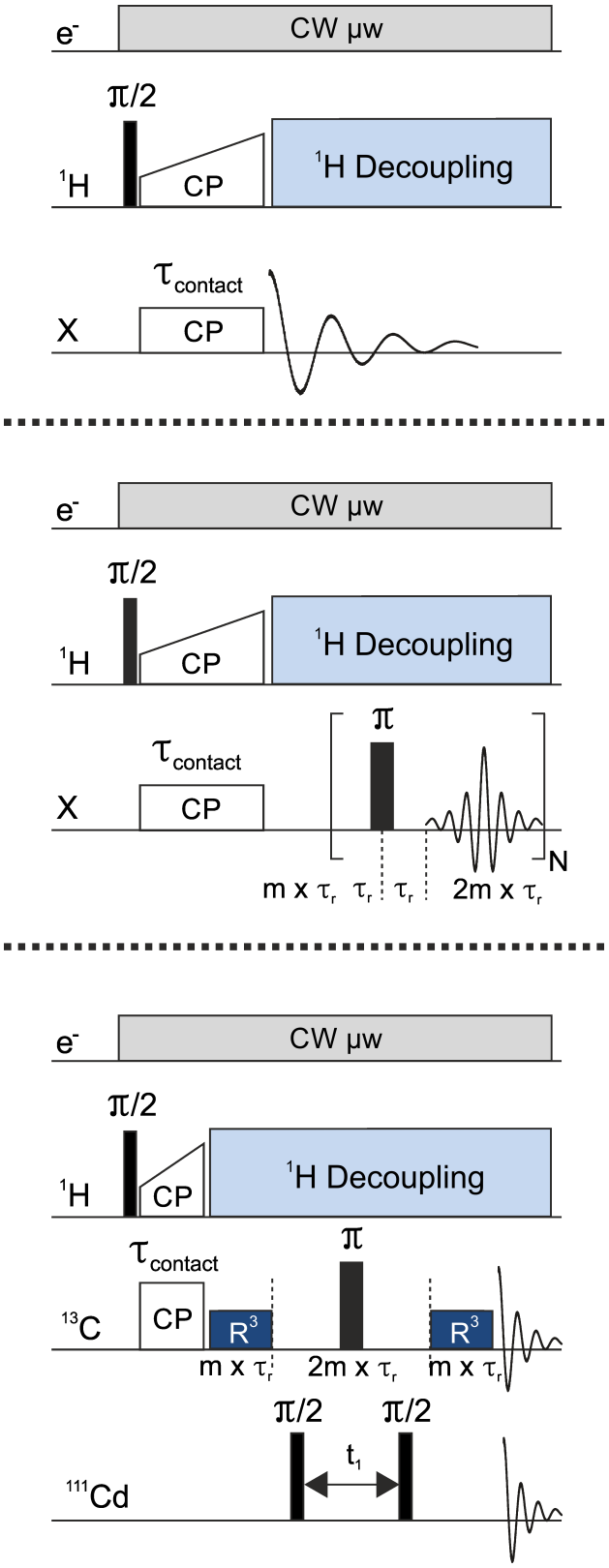

Figure S1. (**top**) Pulse sequences for indirect DNP enhanced CPMAS NMR experiments. Under continuous microwave (CW µw) irradiation, polarization of the electrons is transferred to the protons contained in the sample. The enhanced proton polarization is then transferred to the hetero-nucleus X (X = ^{31}P, ^{77}Se, ^{13}C *etc*.) with CP. The contact time determines the distance of the ^{1}H-X polarization transfer; longer contact times enable polarization of nuclei more distant from the protons. By selecting the contact time of the experiments, NMR signals can be observed from the surface or from nuclei at the surface and in the QD core (see Figure S2 for illustration of this effect).
(**middle**) By using a CP-Carr-Purcell-Meilboom_Gill (CP-CPMG) pulse sequence the signal per transient is increased as inhomogeneous broadening is refocused N-times by pi-pulses and multiple spin echoes are acquired in each transient. The number of spin-echoes which can be acquired depends on the transverse relaxation time (T_2) of the hetero-nucleus. The spikelet pattern, which is obtained by direct Fourier transformation (FT) of the echo train, can be converted to a standard line shape-mode spectrum, by co-adding all of the echoes in the time domain, followed by FT of a single co-added echo. Both processing procedures have been used throughout this work.
(**bottom**) Dipolar Hetero-nuclear Multiple-Quantum Correlation Rotatory Resonance Recoupling (D-HMQC-R^3) pulse sequence[19, 20]. This pulse sequence correlates dipole coupled ^{13}C-^{111}Cd spins.

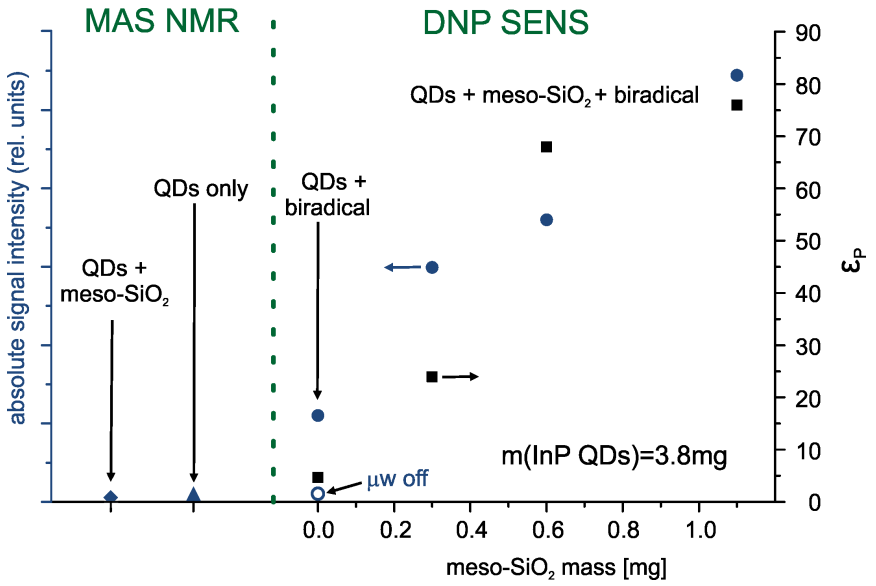

Figure S2. Quantitative comparison of the absolute ^{31}P NMR signal intensities obtained for myristate-capped InP QDs in conventional MAS NMR and in DNP NMR. 7 nm pore meso-SiO_2 was used for DNP NMR. All samples contained 3.8 mg of InP QDs, total TCE content of 20 µL, combined with either or both meso-SiO_2 (0.2-1 mg) and biradical (at a constant final concentration of 16 mM with respect to the TCE volume). Hence samples containing silica had slightly lower InP-per-rotor volume density. Quantitatively, an absolute signal intensity enhancement of 51 was obtained with a DNP enhancement of 80, pointing to effective dilution factor of just 1.5-1.6, fully in agreement with a factor of 1.4 estimated from porosity of 71% (calculated from 0.91 cm^3/g pore volume of 7 nm pore size MSU-H and 2.65 g/cm^3 bulk density of SiO_2). Importantly, the quantity of meso-SiO_2 has to be optimized such that it is just sufficient to absorb the whole amount of QD-biradical solution (1.1 mg of meso-SiO_2 for 3.8 mg of InP QDs, as an example).

Figure S2: myristate-capped InP QDs

12.7 µL of a saturated solution of myristate-capped InP QDs in TCE was mixed with 6.3 µL 50 mM TEKPol in TCE or 6.3 µL of pure TCE on a watch glass yielding 16 mM radical or radical-free solution. Various amount of meso-SiO_2 (7 nm pore size) were impregnated with the (radical-)QD solution and then packed into a 3.2 mm sapphire rotor.

Acquisition parameters for ^{31}P CP DNP NMR	
Magnetic field	9.4 T
Temperature	100 K
Rotor diameter	3.2 mm
Pulse Sequence	CP-echo
Number of scans	128
Recycle delay (s)	1.7
Spectral width (kHz)	100
Spinning frequency (Hz)	8000
Acquisition length (number of points)	2048
^{1}H 90° pulse width [π/2] (µs)	2.5
Contact pulse length (ms)	1.5
^{1}H rf field during contact pulse (kHz)	70
^{31}P rf field during contact pulse (kHz)	68

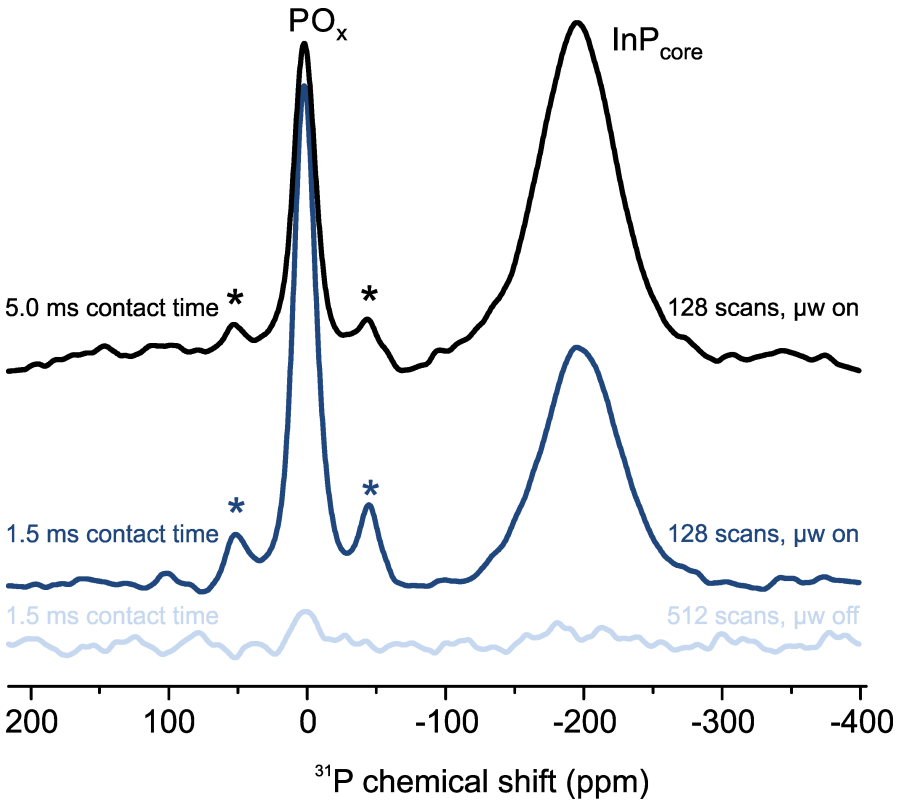

Figure S3. ^{31}P CPMAS DNP NMR spectra of myristate-capped 3 nm InP QDs spectra which were acquired with different CP contact times. All other experimental conditions remained the same. The longer contact time (5.0 ms) enables excitation of ^{31}P nuclei in the core of the QDs which are more distant from the surface ligands.

Figure S3: myristate-capped InP QDs

12.7 μL of a saturated solution of myristate-capped InP QDs in TCE was mixed with 6.3 μL 50 mM TEKPol in TCE on a watch glass yielding a final TEKPol concentration of ca. 16 mM. A minimal amount of meso-SiO_2 (7 nm pore size) was impregnated with the radical-QD solution and then packed into a 3.2 mm sapphire rotor.

Acquisition parameters for ^{31}P CP DNP NMR	
Magnetic field	9.4 T
Temperature	100 K
Rotor diameter	3.2 mm
Pulse Sequence	CP-echo
Number of scans	128
Recycle delay (s)	1.7
Spectral width (kHz)	100
Spinning frequency (Hz)	8000
Acquisition length (number of points)	2048
^{1}H 90° pulse width [π/2] (μs)	2.5
Contact pulse length (ms)	1.5/5
^{1}H rf field during contact pulse (kHz)	70
^{31}P rf field during contact pulse (kHz)	68

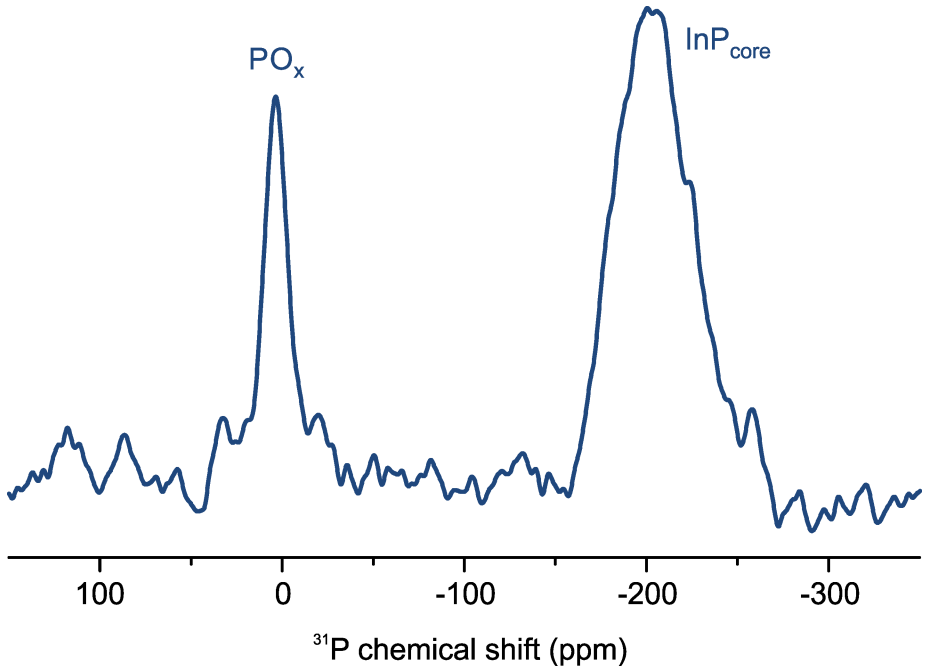

Figure S4. Conventional single-pulse ^{31}P MAS NMR spectrum of myristate-capped 3 nm InP QDs. The single pulse sequence guarantees homogeneous excitation of all phosphorous atoms, independently of their position in or on the QD. By comparing the integrals one can conclude that about a quarter of the phosphorous atoms are localized at the surface of the QDs. 50 mg myristate-capped InP QDs were precipitated with excess of EtOH and dried under vacuum before being filled into a 2.5 mm zirconia rotor. The spectrum was acquired at 11.7 T and 298 K with a 10 s recycle delay.

Acquisition parameters for ^{31}P MAS NMR	
Magnetic field	11.7 T
Temperature	Room temperature
Rotor diameter	2.5 mm
Pulse Sequence	one-pulse
Number of scans	1872
Recycle delay (s)	10
Spectral width (kHz)	156
Spinning frequency (Hz)	20000
Acquisition length (number of points)	2048
^{31}P 90° pulse width [π/2] (μs)	2.8

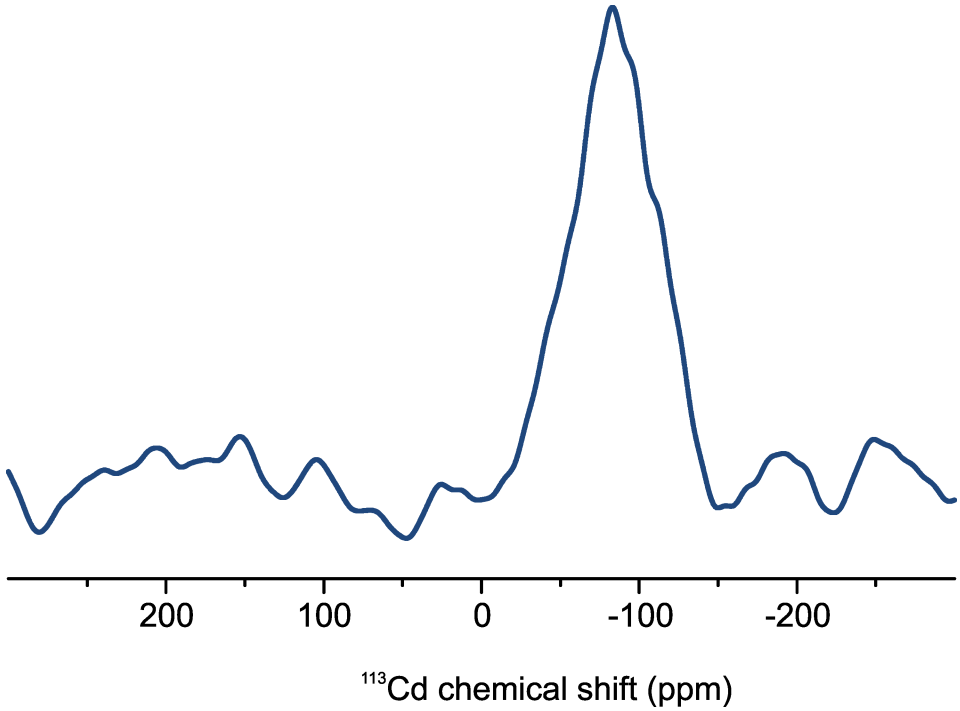

Figure S5. Conventional room temperature single-pulse ^{113}Cd MAS NMR spectrum of oleate-capped 3.5 nm ZB-CdSe QDs. The line shape is dominated by inhomogeneous line broadening, as it is expected for nm-sized structures. 50 mg of CdSe-OA were precipitated with excess of EtOH and vacuum dried before being packed into a 4 mm zirconia rotor. The spectrum was acquired at 16.4 T and 298 K with a 10 s recycle delay and 7408 scans.

Acquisition parameters for ^{113}Cd NMR	
Magnetic field	16.4 T
Temperature	Room temperature
Rotor diameter	4 mm
Pulse Sequence	echo
Number of scans	7408
Recycle delay (s)	10
Spectral width (kHz)	156
Spinning frequency (Hz)	600
Acquisition length (number of points)	4096
^{113}Cd 90° pulse width [π/2] (μs)	4.0

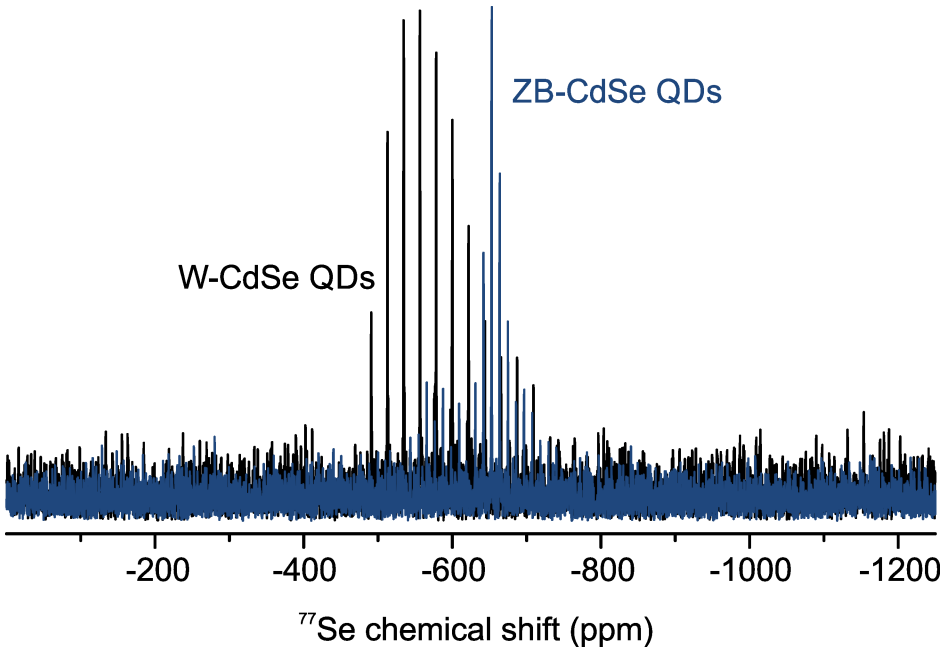

Figure S6. ^{77}Se CP-CPMG DNP NMR spectra of phosphonate-capped WZ-CdSe QDs (black) and oleate-capped ZB-CdSe QDs (dark blue). The chemical shifts of ZB-CdSe (δ = -579, -654) is shifted to higher frequencies compared to W-CdSe (δ = -556 ppm) by 100 ppm. Spectra were acquired using CP-CPMG pulse sequence in order to reduce the total experiment times. Spectra were acquired at 14.1 T and ca. 100 K.

Details for WZ-CdSe QDs. 12.7 µL of a saturated solution of WZ-CdSe QDs in TCE was mixed with 6.3 µL 50 mM TEKPol in TCE on a watch glass yielding a final TEKPol concentration of ca. 16 mM. Minimal amount of meso-SiO_2 (7 nm pore size) was impregnated with the radical-QD solution and then packed into a 3.2 mm sapphire rotor.

Acquisition parameters for ^{77}Se CP-CPMG DNP NMR	
Magnetic field	14.1 T
Temperature	100 K
Rotor diameter	3.2 mm
Pulse Sequence	CP-CPMG
Number of scans	512
Recycle delay (s)	40
Spectral width (kHz)	312
Spinning frequency (Hz)	10000
Acquisition length (number of points)	7596
^{1}H 90° pulse width [π/2] (µs)	2.5
^{77}Se 180° pulse width [π] (µs)	9.0
Number of spin echos	31
Duration of spin echos (µs)	194
Contact pulse length (ms)	9.5
^{1}H rf field during contact pulse (kHz)	100
^{77}Se rf field during contact pulse (kHz)	73

Details for ZB-CdSe QDs. 12.7 µL of a saturated TCE solution of ZB-CdSe capped with ^{13}C-1-oleate ligands was mixed with 6.3 µL 50 mM TEKPol in TCE on a watch glass yielding a final TEKPol concentration of ca. 16 mM. Minimal amount of meso-SiO_2 (15 nm pore size) was impregnated with the radical-QD solution and then packed into a 3.2 mm sapphire rotor.

Acquisition parameters for ^{77}Se CP DNP NMR	
Magnetic field	9.4 T
Temperature	100 K
Rotor diameter	3.2 mm
Pulse Sequence	CP-CPMG
Number of scans	19‘040
Recycle delay (s)	2.7
Spectral width (kHz)	100
Spinning frequency (Hz)	10’000
Acquisition length (number of points)	7650
^{1}H 90° pulse width [π/2] (µs)	2.5
^{77}Se 180° pulse width [π] (µs)	8.6
Number of spin echos	31
Duration of spin echos (ms)	1.000
Contact pulse length (ms)	14.0
^{1}H rf field during contact pulse (kHz)	80
^{77}Se rf field during contact pulse (kHz)	66

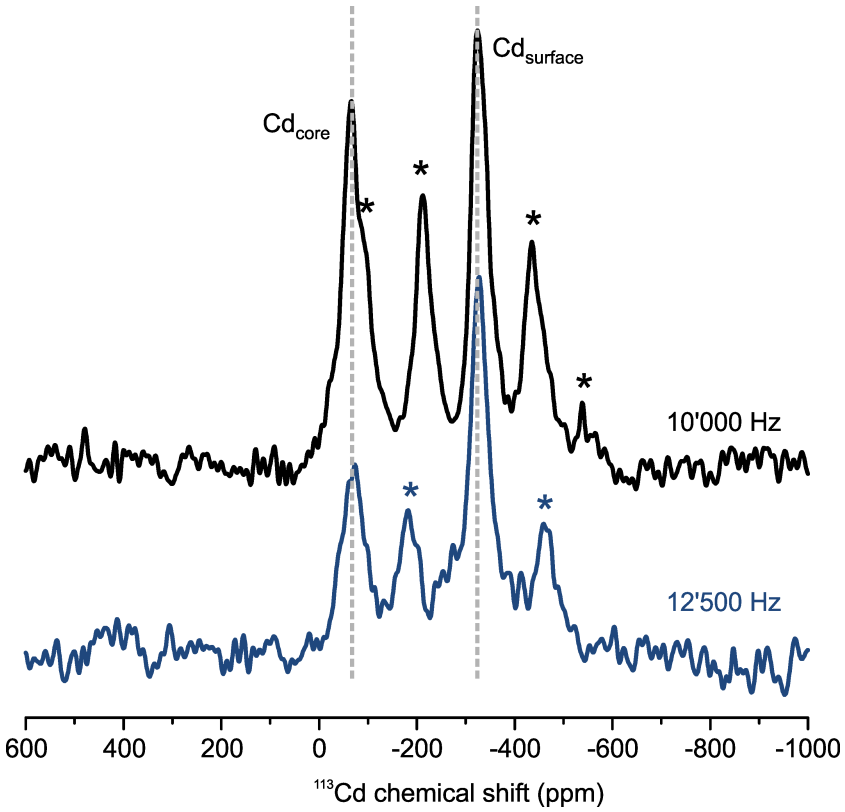

Figure S7. ^{113}Cd CPMAS DNP NMR spectra of ZB-CdSe at different MAS spinning speeds (10000 Hz: upper, black spectrum; 12500 Hz: lower, dark blue spectrum). The peaks remaining at the same chemical shifts, independent of the spinning speed, were identified to be isotropic signals (denoted with dotted grey lines) whereas the spinning side bands (marked with asterisks) are shifted in frequency according to the spinning speeds.

Figure S7: oleate-capped CdSe QDs

12.7 µL of a saturated solution of ZB-CdSe in TCE was mixed with 6.3 µL 50 mM TEKPol in TCE on a watch glass yielding 16 mM radical solution. Minimal amount of meso-SiO_2 (15 nm pore size) was impregnated with the radical-QD solution and then packed into a 3.2 mm sapphire rotor.

Acquisition parameters for ^{77}Se CP DNP NMR	
Magnetic field	9.4 T
Temperature	100 K
Rotor diameter	3.2 mm
Pulse Sequence	CP-echo
Number of scans	8192/2240
Recycle delay (s)	3.8
Spectral width (kHz)	150
Spinning frequency (Hz)	10000/12500
Acquisition length (number of points)	1024
^{1}H 90° pulse width [π/2] (µs)	2.5
Contact pulse length (ms)	1.5
^{1}H rf field during contact pulse (kHz)	80
^{77}Se rf field during contact pulse (kHz)	66

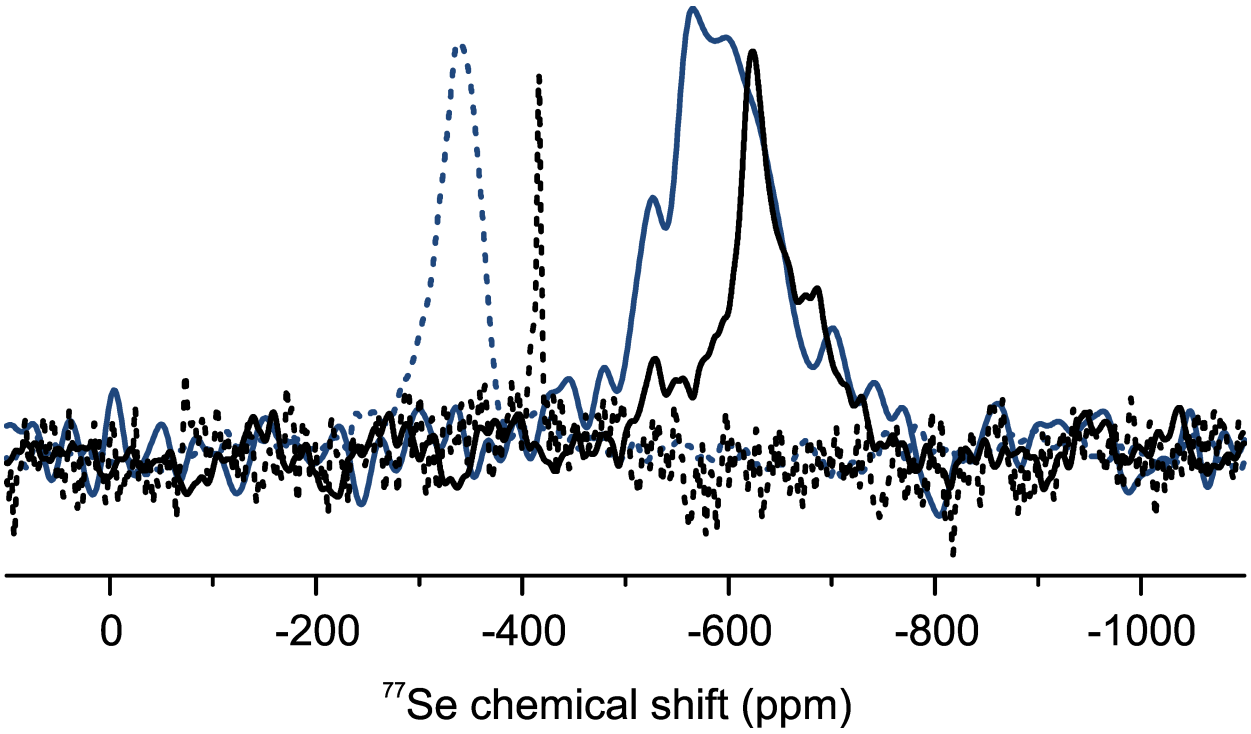

Figure S8. NMR spectra summarizing chemical shifts of all ^{77}Se containing species involved in the preparation of selenide-capped CdSe QDs. All spectra were measured at 100 K except the one of K_2Se powder which was acquired at ca. 298 K. Oleate-capped ZB-CdSe QDs (black, solid line, -623 ppm) and selenide-capped ZB-CdSe QDs (dark blue, solid line, -565 ppm) spectra were acquired with DNP enhancement. K_2Se dissolved in FA (dark blue, dotted line, -339 ppm) and K_2Se powder (black, dotted-line, -416 ppm) spectra were obtained with conventional NMR spectroscopy without μw irradiation.

Details for K_2Se solution in FA. 1.3 mg of K_2Se in 20 μL FA were filled into a 3.2 mm sapphire rotor.

Acquisition parameters for ^{77}Se NMR	
Magnetic field	14.1
Temperature	100 K
Rotor diameter	3.2 mm
Pulse Sequence	CP-echo
Number of scans	4048
Recycle delay (s)	2.2
Spectral width (kHz)	312
Spinning frequency (Hz)	10’000
Acquisition length (number of points)	1496
^{1}H 90° pulse width [π/2] (μs)	2.5
Contact pulse length (ms)	9.5
^{1}H rf field during contact pulse (kHz)	100
^{77}Se rf field during contact pulse (kHz)	73

Details for K_2Se powder. K_2Se powder was filled into 2.5mm rotor under inert atmosphere.

Acquisition parameters for ^{77}Se NMR	
Magnetic field	14.1 T
Temperature	Room temperature
Rotor diameter	2.5 mm
Pulse Sequence	30° one-pulse
Number of scans	577
Recycle delay (s)	300 s
Spectral width (kHz)	20.8
Spinning frequency (Hz)	20000
Acquisition length (number of points)	2048
^{77}Se 90° pulse width [π/2] (μs)	100

Details for selenide-capped ZB-CdSe QDs. In a glovebox, 30 μL of selenide-capped ZB-CdSe QD solution in FA was absorbed by minimal amount of meso-SiO_2 (15 nm pore size) after which the solvent was evaporated by applying vacuum. This was repeated a second time in order to increase QD concentration within the meso-SiO_2. The resulting dark red powder was then impregnated with 20 μL 16 mM TEKPol solution in TCE and packed into a 3.2 mm sapphire rotor.

Acquisition parameters for ^{77}Se CP-CPMG DNP NMR	
Magnetic field	9.4 T
Temperature	100 K
Rotor diameter	3.2 mm
Pulse Sequence	CP-CPMG
Number of scans	2712
Recycle delay (s)	20
Spectral width (kHz)	100
Spinning frequency (Hz)	10000
Acquisition length (number of points)	7650
^{1}H 90° pulse width [π/2] (μs)	2.5
^{77}Se 180° pulse width [π] (μs)	8.6
Number of spin echos	31
Duration of spin echos (ms)	1.000
Contact pulse length (ms)	14.0
^{1}H rf field during contact pulse (kHz)	80
^{77}Se rf field during contact pulse (kHz)	66

Details for oleate-capped ZB-CdSe QDs. 12.7 µL of a saturated TCE solution of ZB-CdSe QDs capped with ^{13}C-1-oleate was mixed with 6.3 µL 50 mM TEKPol in TCE on a watch glass yielding 16 mM radical solution. A minimal amount of meso-SiO_2 (15 nm pore size) was impregnated with the radical-QD solution and then packed into a 3.2 mm sapphire rotor.

Acquisition parameters for ^{77}Se CP-CPMG DNP NMR	
Magnetic field	9.4 T
Temperature	100 K
Rotor diameter	3.2 mm
Pulse Sequence	CP-CPMG
Number of scans	19‘040
Recycle delay (s)	2.7
Spectral width (kHz)	100
Spinning frequency (Hz)	10000
Acquisition length (number of points)	7650
^{1}H 90° pulse width [π/2] (µs)	2.5
^{77}Se 180° pulse width [π] (µs)	8.6
Number of spin echos	31
Duration of spin echos (ms)	1.000
Contact pulse length (ms)	14.0
^{1}H rf field during contact pulse (kHz)	80
^{77}Se rf field during contact pulse (kHz)	66

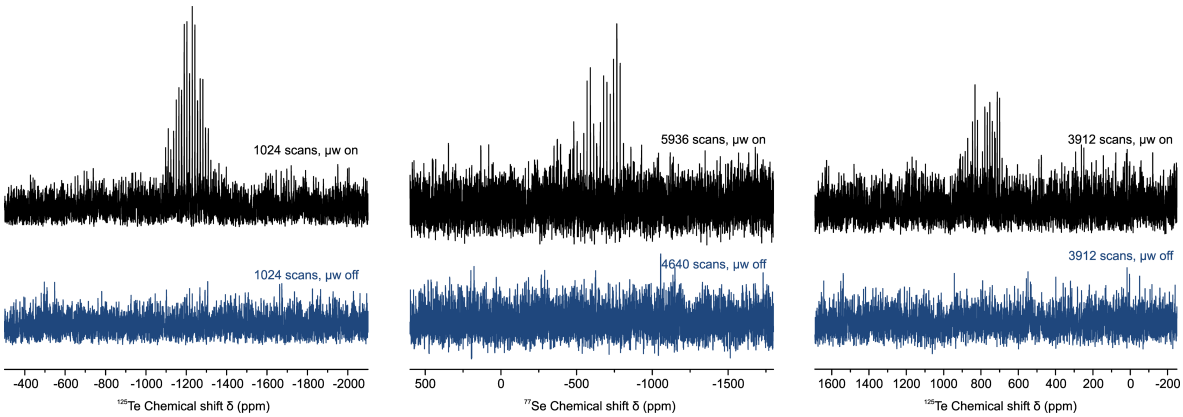

Figure S9. DNP NMR spectra of oleate-capped CdTe (left), PbSe (middle) and PbTe (right) QDs. These ^{77}Se and ^{125}Te spectra illustrate the range of NMR-active elements and QDs accessible to DNP NMR. The ^{125}Te and ^{77}Se NMR signals of CdTe and PbSe, respectively, were observed in the range where bulk signals have been reported[21, 22]. PbSe QDs were handled in inert atmosphere and do not feature any oxidation of the surface. CdTe QDs are not oxidized even after prolonged storage under ambient conditions. For PbTe no ^{125}Te NMR signal could be observed at the reported chemical shift of bulk PbTe.[23] However, the chemical shift of the ^{125}Te NMR signal was found in the frequency range where tellurium oxides are found. This observation is explained by the full oxidation of the PbTe-surface despite careful handling in inert atmosphere.

Details for oleate-capped CdTe QDs. 12.7 µL of a saturated TCE solution of oleate-capped CdTe QDs was mixed with 6.3 µL 50 mM TEKPol in TCE on a watch glass yielding a 16 mM radical solution. Minimal amounts of meso-SiO_2 (30 nm pore size) were impregnated with the radical-QD solution and then packed into a 3.2 mm sapphire rotor.

Acquisition parameters for ^{77}Se CP-CPMG DNP NMR	
Magnetic field	14.1 T
Temperature	100 K
Rotor diameter	3.2 mm
Pulse Sequence	CP-CPMG
Number of scans	1024
Recycle delay (s)	4.2
Spectral width (kHz)	375
Spinning frequency (Hz)	10000
Acquisition length (number of points)	9098
^{1}H 90° pulse width [π/2] (µs)	2.5
^{77}Se 180° pulse width [π] (µs)	15.0
Number of spin echos	31
Duration of spin echos (µs)	194
Contact pulse length (ms)	6.0
^{1}H rf field during contact pulse (kHz)	100
^{77}Se rf field during contact pulse (kHz)	73

Details for oleate-capped PbSe QDs. In a glovebox, 5mg of dried oleate-capped PbSe QDs were redispersed in 15 μL 16 mM TEKPol in TCE. Minimal amount of meso-SiO_2 (7 nm pore size) was impregnated with the radical-QD solution and then packed into a 3.2 mm sapphire rotor.

Acquisition parameters for ^{77}Se CP-CPMG DNP NMR	
Magnetic field	14.1 T
Temperature	100 K
Rotor diameter	3.2 mm
Pulse Sequence	CP-CPMG
Number of scans	5936
Recycle delay (s)	15
Spectral width (kHz)	312
Spinning frequency (Hz)	10000
Acquisition length (number of points)	7596
^{1}H 90° pulse width [π/2] (μs)	2.5
^{77}Se 180° pulse width [π] (μs)	9.0
Number of spin echos	31
Duration of spin echos (μs)	194
Contact pulse length (ms)	9.5
^{1}H rf field during contact pulse (kHz)	100
^{77}Se rf field during contact pulse (kHz)	73

Details for oleate-capped PbTe QDs. In a glovebox, 5mg of dried oleate-capped PbTe QDs were redispersed in 15 μL 16 mM TEKPol in TCE. Minimal amount of meso-SiO_2 (7 nm pore size) was impregnated with the radical-QD solution and then packed into a 3.2 mm sapphire rotor.

Acquisition parameters for ^{77}Se CP-CPMG DNP NMR	
Magnetic field	14.1 T
Temperature	100 K
Rotor diameter	3.2 mm
Pulse Sequence	CP-CPMG
Number of scans	3912
Recycle delay (s)	3.3
Spectral width (kHz)	375
Spinning frequency (Hz)	10000
Acquisition length (number of points)	9098
^{1}H 90° pulse width [π/2] (μs)	2.5
^{77}Se 180° pulse width [π] (μs)	15.0
Number of spin echos	31
Duration of spin echos (μs)	194
Contact pulse length (ms)	6.0
^{1}H rf field during contact pulse (kHz)	100
^{77}Se rf field during contact pulse (kHz)	73

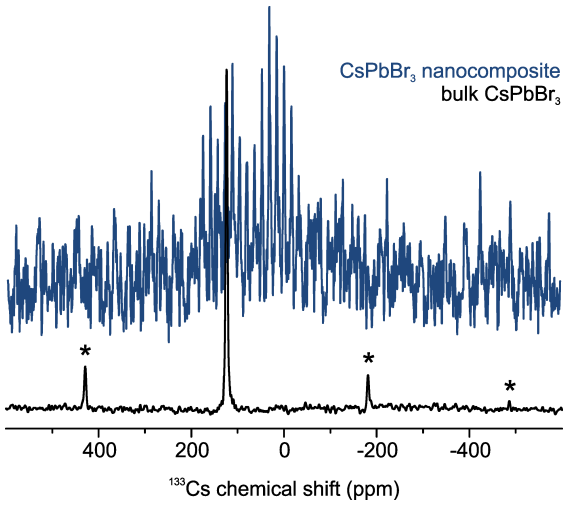

Figure S10. ^{133}Cs DNP NMR spectrum of $CsPbBr_3$/meso-SiO_2 nanocomposite (dark blue). A conventional single-pulse MAS NMR spectrum of bulk $CsPbBr_3$ is presented for comparison. The quadrupole moment and the CSA broaden the signal of the surface Cs atoms. Spinning side bands are marked with asterisks.

Details for $CsPbBr_3$/meso-SiO_2 nanocomposite. 10 µL of 16 mM TEKPol solution in TCE was soaked into $CsPbBr_3$/meso-SiO_2 powder and then filled into 3.2 mm sapphire rotor.

Acquisition parameters for ^{133}Cs CP-CPMG DNP NMR	
Magnetic field	14.1 T
Temperature	100 K
Rotor diameter	3.2 mm
Pulse Sequence	CP-CPMG
Number of scans	7424
Recycle delay (s)	14.3
Spectral width (kHz)	94
Spinning frequency (Hz)	10000
Acquisition length (number of points)	3100
^{1}H 90° pulse width [π/2] (µs)	2.5
Contact pulse length (ms)	4.0
^{1}H rf field during contact pulse (kHz)	100
^{133}Cs rf field during contact pulse (kHz)	68

Details for bulk $CsPbBr_3$. Bulk $CsPbBr_3$ powder was packed into a 2.5 mm zirconia rotor.

Acquisition parameters for ^{133}Cs NMR	
Magnetic field	11.7 T
Temperature	Room temperature
Rotor diameter	2.5 mm
Pulse Sequence	echo
Number of scans	1
Recycle delay (s)	90
Spectral width (kHz)	132
Spinning frequency (Hz)	20’000
Acquisition length (number of points)	5248
^{113}Cs 90° pulse width [π/2] (µs)	3.5

VII. Details for all NMR experiments presented in main text

Figure 2d: myristate-capped InP QDs

12.7 µL of a saturated myristate-capped InP QD solution in TCE was mixed with 6.3 µL 50 mM TEKPol in TCE directly inside a sapphire 3.2 mm rotor which was sealed with one-way silicon plug.

Acquisition parameters for ^{31}P CP DNP NMR	
Magnetic field	9.4 T
Temperature	100 K
Rotor diameter	3.2 mm
Pulse Sequence	CP-echo
Number of scans	128/512
Recycle delay (s)	1.7
Spectral width (kHz)	100
Spinning frequency (Hz)	8000
Acquisition length (number of points)	2048
^{1}H 90° pulse width [π/2] (µs)	2.5
Contact pulse length (ms)	1.5
^{1}H rf field during contact pulse (kHz)	70
^{31}P rf field during contact pulse (kHz)	68

Figure 2e and f: myristate-capped InP QDs

12.7 µL of a saturated myristate-capped InP QD solution in TCE was mixed with 6.3 µL 50 mM TEKPol in TCE on a watch glass yielding 16 mM radical solution. Minimal amount of meso-SiO_2 (7 nm pores for center bottom, for right indicated in the plot) was impregnated with the radical-QD solution and then packed into a 3.2 mm sapphire rotor.

Acquisition parameters for ^{31}P CP DNP NMR	
Magnetic field	9.4 T
Temperature	100 K
Rotor diameter	3.2 mm
Pulse Sequence	CP-echo
Number of scans	128/512
Recycle delay (s)	1.7
Spectral width (kHz)	100
Spinning frequency (Hz)	8000
Acquisition length (number of points)	2048
^{1}H 90° pulse width [π/2] (µs)	2.5
Contact pulse length (ms)	1.5
^{1}H rf field during contact pulse (kHz)	70
^{31}P rf field during contact pulse (kHz)	68

Figure 3a: oleate-capped ZB-CdSe QDs

12.7 µL of a saturated solution of oleate-capped CdSe QDs in TCE was mixed with 6.3 µL 50 mM TEKPol in TCE on a watch glass yielding 16 mM radical solution. Minimal amount of meso-SiO_2 (15 nm pore size) was impregnated with the radical-QD solution and then packed into a 3.2 mm sapphire rotor.

Acquisition parameters for ^{113}Cd CP DNP NMR	
Magnetic field	9.4 T
Temperature	100 K
Rotor diameter	3.2 mm
Pulse Sequence	CP-echo/CP/CP
Number of scans	8192/1524/1188
Recycle delay (s)	3.8
Spectral width (kHz)	150/100/100
Spinning frequency (Hz)	10000/8000/8000
Acquisition length (number of points)	1024/512/512
^{1}H 90° pulse width [π/2] (µs)	2.5
^{113}Cd 90° pulse width [π/2] (µs)	8
Contact pulse length (ms)	15
^{1}H rf field during contact pulse (kHz)	78
^{113}Cd rf field during contact pulse (kHz)	62

Figure 3b: ^{13}C-1-oleate-capped ZB-CdSe QDs

12.7 µL of a saturated solution of CdSe QDs in TCE capped with ^{13}C-labeled oleate was mixed with 6.3 µL 50 mM TEKPol in TCE on a watch glass yielding 16 mM radical solution. Minimal amount of meso-SiO_2 (15 nm pore size) was impregnated with the radical-QD solution and then packed into a 3.2 mm sapphire rotor.

Acquisition parameters for ^{77}Se CP-CPMG DNP NMR	
Magnetic field	9.4 T
Temperature	100 K
Rotor diameter	3.2 mm
Pulse Sequence	CP-CPMG
Number of scans	19040/1524/1188
Recycle delay (s)	2.7
Spectral width (kHz)	100
Spinning frequency (Hz)	10000
Acquisition length (number of points)	7650
^{1}H 90° pulse width [π/2] (µs)	2.5
^{77}Se 180° pulse width [π] (µs)	8.6
Number of spin echos	31
Duration of spin echos (ms)	1.000
Contact pulse length (ms)	14
^{1}H rf field during contact pulse (kHz)	72
^{77}Se rf field during contact pulse (kHz)	65

Figure 3c: ^{13}C-1-oleate-capped ZB-CdSe QDs

12.7 µL of a saturated solution of CdSe QDs in TCE capped with ^{13}C-labeled oleate was mixed with 6.3 µL 50 mM TEKPol in TCE on a watch glass yielding 16 mM radical solution. Minimal amount of meso-SiO_2 (15 nm pore size) was impregnated with the radical-QD solution and then packed into a 3.2 mm sapphire rotor.

Acquisition parameters for ^{13}C CP DNP NMR	
Magnetic field	9.4 T
Temperature	100 K
Rotor diameter	3.2 mm
Pulse Sequence	CP
Number of scans	32/512
Recycle delay (s)	2.7
Spectral width (kHz)	25
Spinning frequency (Hz)	9000
Acquisition length (number of points)	512
^{1}H 90° pulse width [π/2] (µs)	2.5
Contact pulse length (ms)	2200
^{1}H rf field during contact pulse (kHz)	72
^{13}C rf field during contact pulse (kHz)	55

Figure 4: ^{13}C-1-oleate-capped ZB-CdSe QDs

12.7 µL of a saturated solution of CdSe QDs in TCE capped with ^{13}C-labeled oleate was mixed with 6.3 µL 50 mM TEKPol in TCE on a watch glass yielding 16 mM radical solution. Minimal amount of meso-SiO_2 (15 nm pore size) was impregnated with the radical-QD solution and then packed into a 3.2 mm sapphire rotor.

Acquisition parameters for ^{13}C-^{111}Cd D-HMQC DNP	
Magnetic field	9.4 T
Temperature	100 K
Rotor Diameter	3.2 mm
Pulse Sequence	D-HMQC
t1 increment (µs)	4
Number of t1 increment	48
Number of scans per t1 increment	400
Recycle delay (s)	2.7
Spectral width (kHz)	10
Spinning frequency (Hz)	9000
Acquisition length (number of points)	400
^{1}H 90° pulse width [π/2] (µs)	2.5
^{111}Cd 90° pulse width [π/2] (µs)	2.8
^{13}C 90° pulse width [π/2] (µs)	6.5
^{13}C R^3 recoupling power (Hz)	9000
Contact pulse length (ms)	2.200
^{1}H rf field during contact pulse (kHz)	72
^{13}C rf field during contact pulse (kHz)	55
^{1}H rf field during decoupling (kHz)	100

Figure 5a: selenide-capped ZB-CdSe QDs

30 µL of a selenide-capped ZB-CdSe QD solution in FA was absorbed by minimal amount of meso-SiO_2 (15 nm pore size), followed by the vacuum-evaporation of the solvent. This was repeated a second time in order to increase QD concentration within the meso-SiO_2. The dark red powder was impregnated with 20 µL 16 mM TEKPol solution in TCE and packed into a 3.2 mm sapphire rotor. All the preparation was done in glove box.

Acquisition parameters for ^{77}Se CP-CPMG DNP NMR	
Magnetic field	9.4 T
Temperature	100 K
Rotor diameter	3.2 mm
Pulse Sequence	CP-CPMG
Number of scans	2712
Recycle delay (s)	20
Spectral width (kHz)	100
Spinning frequency (Hz)	10000
Acquisition length (number of points)	7650
^{1}H 90° pulse width [π/2] (µs)	2.5
^{77}Se 180° pulse width [π] (µs)	8.6
Number of spin echos	31
Duration of spin echos (ms)	1.000
Contact pulse length (ms)	14.0
^{1}H rf field during contact pulse (kHz)	80
^{77}Se rf field during contact pulse (kHz)	66

Figure 5b: sulfide-capped InP QDs

10 µL of a saturated sulfide-capped InP QD solution in DMSO-d^6/water (6:4) was mixed with 10 µL 16 mM AMUPol in DMSO-d^6/D_2O/H_2O (15:9:1 by volume) on a watch glass yielding 8 mM radical solution. Minimal amount of meso-SiO_2 (15 nm pore size) was impregnated with the radical-QD solution and then packed into a 3.2 mm sapphire rotor.

Acquisition parameters ^{31}P CP DNP NMR	
Magnetic field	14.1 T
Temperature	100 K
Rotor diameter	3.2 mm
Pulse Sequence	CP-echo
Number of scans	1392
Recycle delay (s)	3.9
Spectral width (kHz)	22
Spinning frequency (Hz)	10000
Acquisition length (number of points)	682
^{1}H 90° pulse width [π/2] (µs)	2.6
Contact pulse length (ms)	1.5
^{1}H rf field during contact pulse (kHz)	96
^{31}P rf field during contact pulse (kHz)	69

Figure 5c: sulfide-capped InP QDs

Minimal amount of meso-SiO_2 (15 nm pore size) was impregnated with 20 µL of a saturated sulfide-capped InP QD solution in FA. The FA was mostly evaporated under vacuum overnight. 15 µL 16 mM TEKPol solution in TCE was then soaked into the QD containing meso-SiO_2, and the entire sample was transferred into a 3.2 mm sapphire rotor.

Acquisition parameters ^{31}P CP DNP NMR	
Manetic field	14.1 T
Temperature	100 K
Rotor diameter	3.2 mm
Pulse Sequence	CP-echo
Number of scans	5088/1392/1392
Recycle delay (s)	7.4
Spectral width (kHz)	22
Spinning frequency (Hz)	10000
Acquisition length (number of points)	682
^{1}H 90° pulse width [π/2] (µs)	2.6
Contact pulse length (ms)	1.5
^{1}H rf field during contact pulse (kHz)	96
^{31}P rf field during contact pulse (kHz)	69

VIII. Supplementary references

1. McCarthy, T. J.; Ngeyi, S. P.; Liao, J. H.; DeGroot, D. C.; Hogan, T.; Kannewurf, C. R.; Kanatzidis, M. G. *Chem. Mat.* **1993,** 5, 331-340.
2. Zagdoun, A.; Casano, G.; Ouari, O.; Schwarzwälder, M.; Rossini, A. J.; Aussenac, F.; Yulikov, M.; Jeschke, G.; Copéret, C.; Lesage, A.; Tordo, P.; Emsley, L. *J. Am. Chem. Soc.* **2013,** 135, 12790-12797.
3. Sauvée, C.; Rosay, M.; Casano, G.; Aussenac, F.; Weber, R. T.; Ouari, O.; Tordo, P. *Angew. Chem.* **2013,** 125, 11058-11061.
4. Grüning, W. R.; Siddiqi, G.; Safonova, O. V.; Copéret, C. *Adv. Synth. Catal.* **2014,** 356, 673-679.
5. Kruk, M. *Acc. Chem. Res.* **2012,** 45, 1678-1687.
6. Xie, R.; Battaglia, D.; Peng, X. *J. Am. Chem. Soc.* **2007,** 129, 15432-15433.
7. Chen, O.; Chen, X.; Yang, Y.; Lynch, J.; Wu, H.; Zhuang, J.; Cao, Y. C. *Angew. Chem. Int. Ed.* **2008,** 47, 8638-8641.
8. Panthani, M. G.; Kurley, J. M.; Crisp, R. W.; Dietz, T. C.; Ezzyat, T.; Luther, J. M.; Talapin, D. V. *Nano Lett.* **2014,** 14, 670-675.
9. Chen, O.; Zhao, J.; Chauhan, V. P.; Cui, J.; Wong, C.; Harris, D. K.; Wei, H.; Han, H.-S.; Fukumura, D.; Jain, R. K.; Bawendi, M. G. *Nat. Mater.* **2013,** 12, 445-451.
10. Kovalenko, M. V.; Talapin, D. V.; Loi, M. A.; Cordella, F.; Hesser, G.; Bodnarchuk, M. I.; Heiss, W. *Angew. Chem. Int. Ed.* **2008,** 47, 3029-3033.
11. Urban, J. J.; Talapin, D. V.; Shevchenko, E. V.; Murray, C. B. *J. Am. Chem. Soc.* **2006,** 128, 3248-3255.
12. Stoumpos, C. C.; Malliakas, C. D.; Peters, J. A.; Liu, Z.; Sebastian, M.; Im, J.; Chasapis, T. C.; Wibowo, A. C.; Chung, D. Y.; Freeman, A. J.; Wessels, B. W.; Kanatzidis, M. G. *Cryst. Growth Des.* **2013,** 13, 2722-2727.
13. Harris, R. K.; Becker, E. D.; Cabral De Menezes, S. M.; Granger, P.; Hoffman, R. E.; Zilm, K. W. *Solid State Nuc. Mag. Res.* **2008,** 33, 41-56.
14. Duncan, T. M., *A Compilation Of Chemical Shift Anisotropies*. Farragut Press: 1990; p 157.
15. Rosay, M.; Tometich, L.; Pawsey, S.; Bader, R.; Schauwecker, R.; Blank, M.; Borchard, P. M.; Cauffman, S. R.; Felch, K. L.; Weber, R. T.; Temkin, R. J.; Griffin, R. G.; Maas, W. E. *Phys. Chem. Chem. Phys.* **2010,** 12, 5850-5860.
16. Pines, A.; Gibby, M. G.; Waugh, J. S. *The Journal of Chemical Physics* **1973,** 59, 569-590.
17. Peersen, O. B.; Wu, X. L.; Kustanovich, I.; Smith, S. O. *J. Magn. Reson. A* **1993,** 104, 334-339.
18. Fung, B. M.; Khitrin, A. K.; Ermolaev, K. *J. Magn. Reson.* **2000,** 142, 97-101.
19. Gan, Z.; Amoureux, J. P.; Trébosc, J. *Chem. Phys. Lett.* **2007,** 435, 163-169.
20. Trebosc, J.; Hu, B.; Amoureux, J. P.; Gan, Z. *J. Magn. Reson.* **2007,** 186, 220-227.
21. Balz, R.; Haller, M.; Hertler, W. E.; Lutz, O.; Nolle, A.; Schafitel, R. *J. Magn. Reson.* **1980,** 40, 9-16.
22. Ratcliffe, C. I.; Yu, K.; Ripmeester, J. A.; Badruz Zaman, M.; Badarau, C.; Singh, S. *Phys. Chem. Chem. Phys.* **2006,** 8, 3510-3519.
23. Taylor, R. E.; Alkan, F.; Koumoulis, D.; Lake, M. P.; King, D.; Dybowski, C.; Bouchard, L.-S. *J. Phys. Chem. C* **2013,** 117, 8959-8967.